13th Summer School on SCIENTIFIC VISUALIZATION

Quantitative descriptors of arterial flows

Diego Gallo – diego.gallo@polito.it
Department of Mechanics and Aerospace Engineering,
Politecnico di Torino

CINECA

OUTLINE

- History & rationale for the visualization of complex arterial flows
- Clinical motivations
- Wall Shear Stress descriptors
- Bulk flow descriptors
- Examples of applications in Computational Fluid Dynamics
- Examples of applications in *in vivo* imaging

Medical images: from form…

Visualizations are meant to facilitate **a better understanding at the conceptual level** and to **open new venues of scientific investigation**. Visual representations moved from the representation of the shape and location of arteries to the attempt to understand causes and consequences of alterations in blood dynamics.

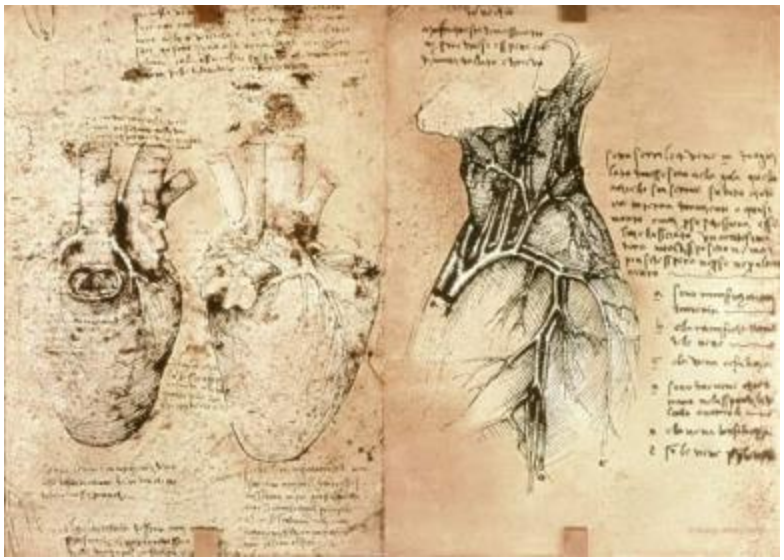

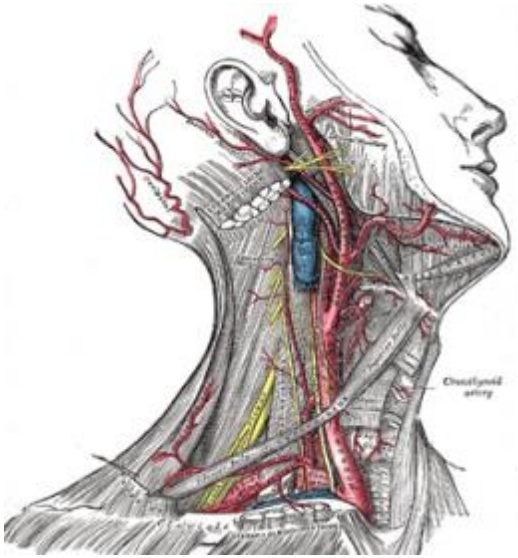

[Leonardo Da Vinci, Vesalius *De Corporis Fabrica*, Grey 1918]

…to function:
How to conceptualize the physical phenomena?

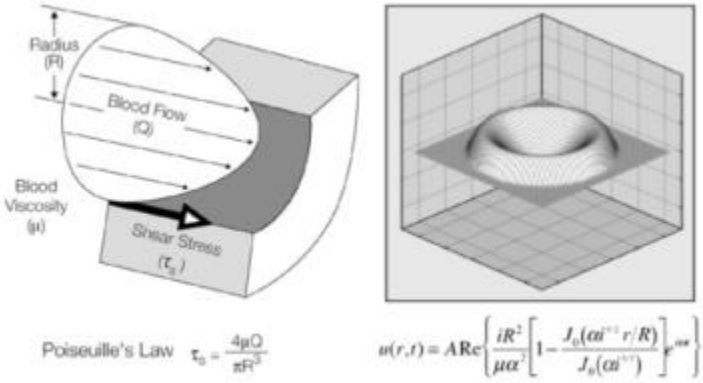

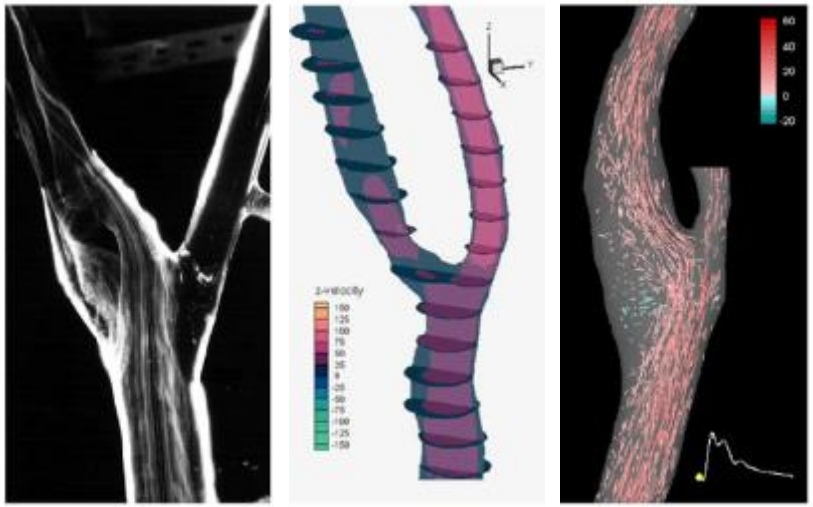

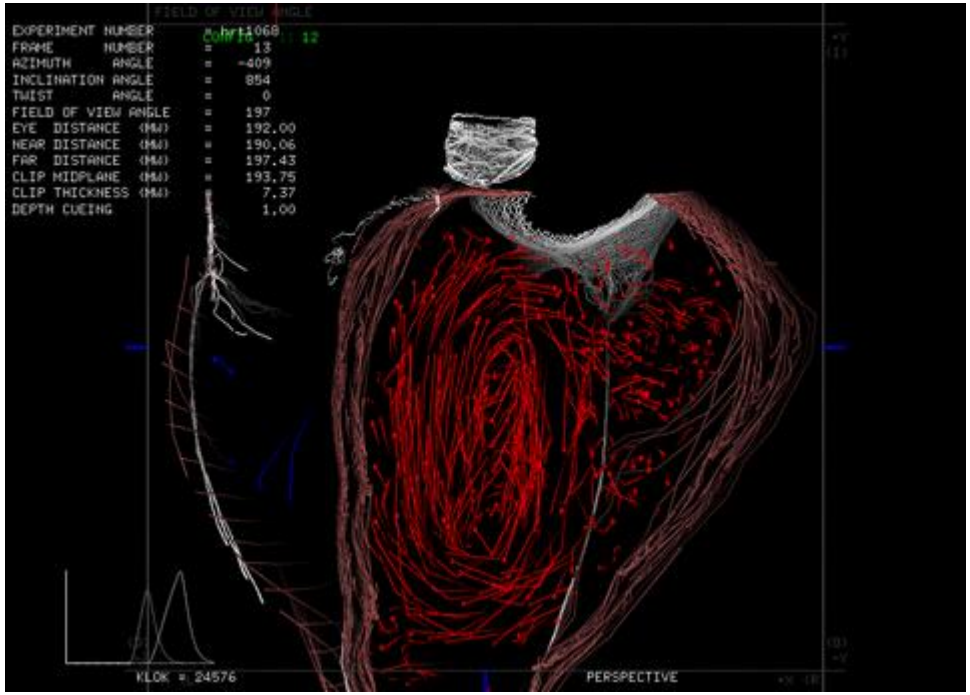

[Peskin et al., 2005]

…to function:
How to conceptualize the physical phenomena?

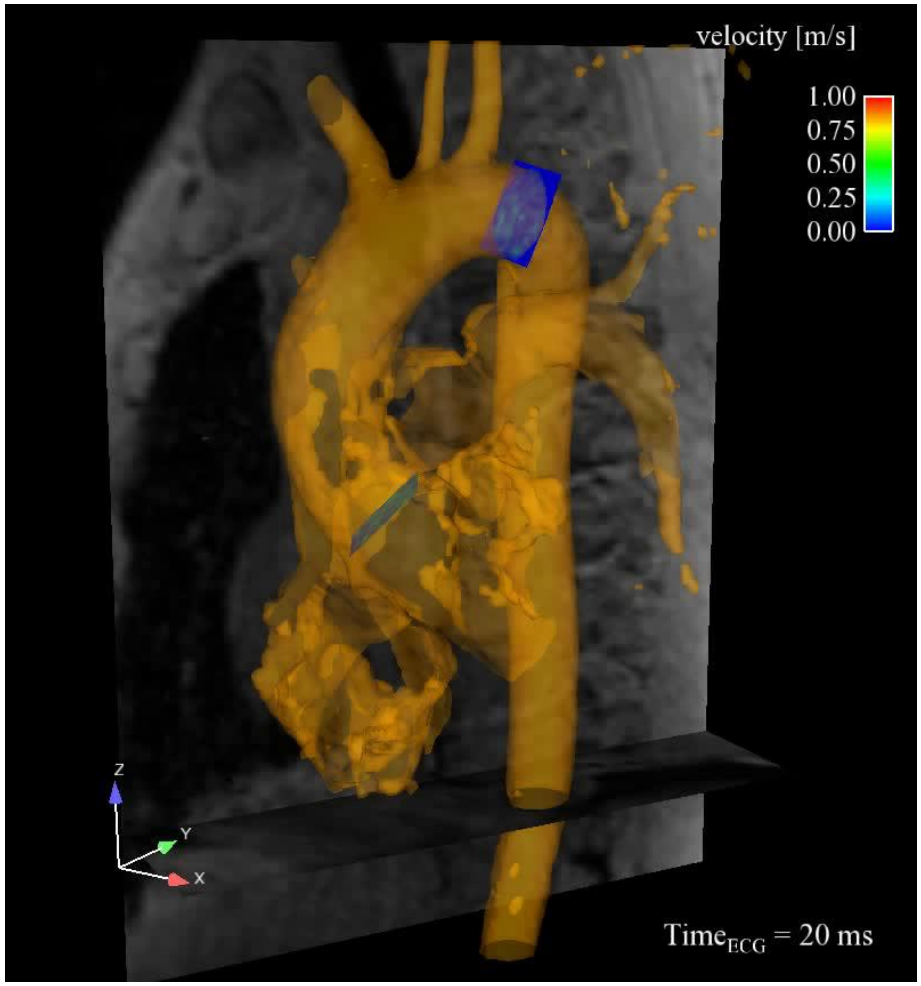

[Markl et al., 2011]

Challenges in virtual imaging

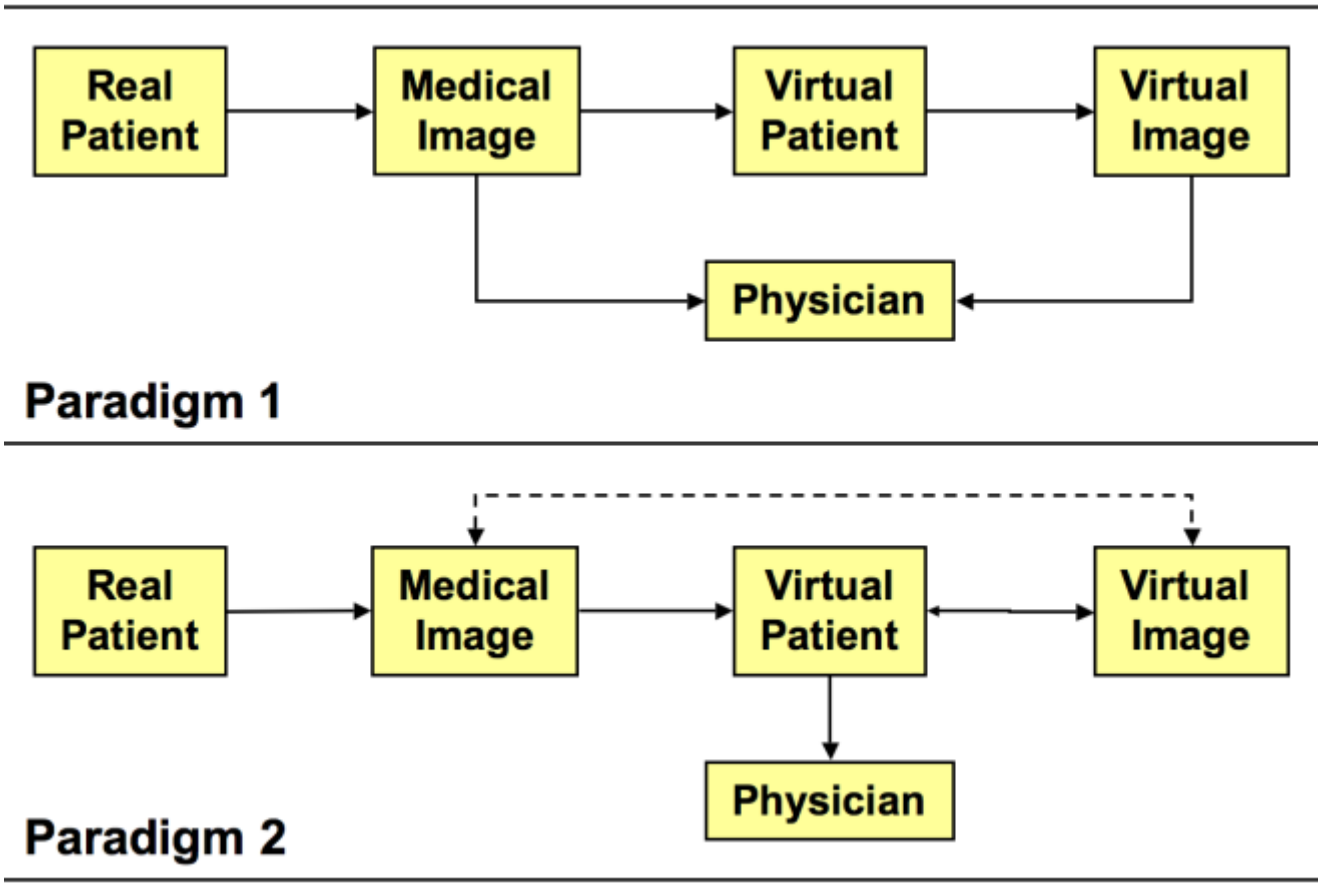

[Steinman & Steinman, 2003]

Visualization Pipeline

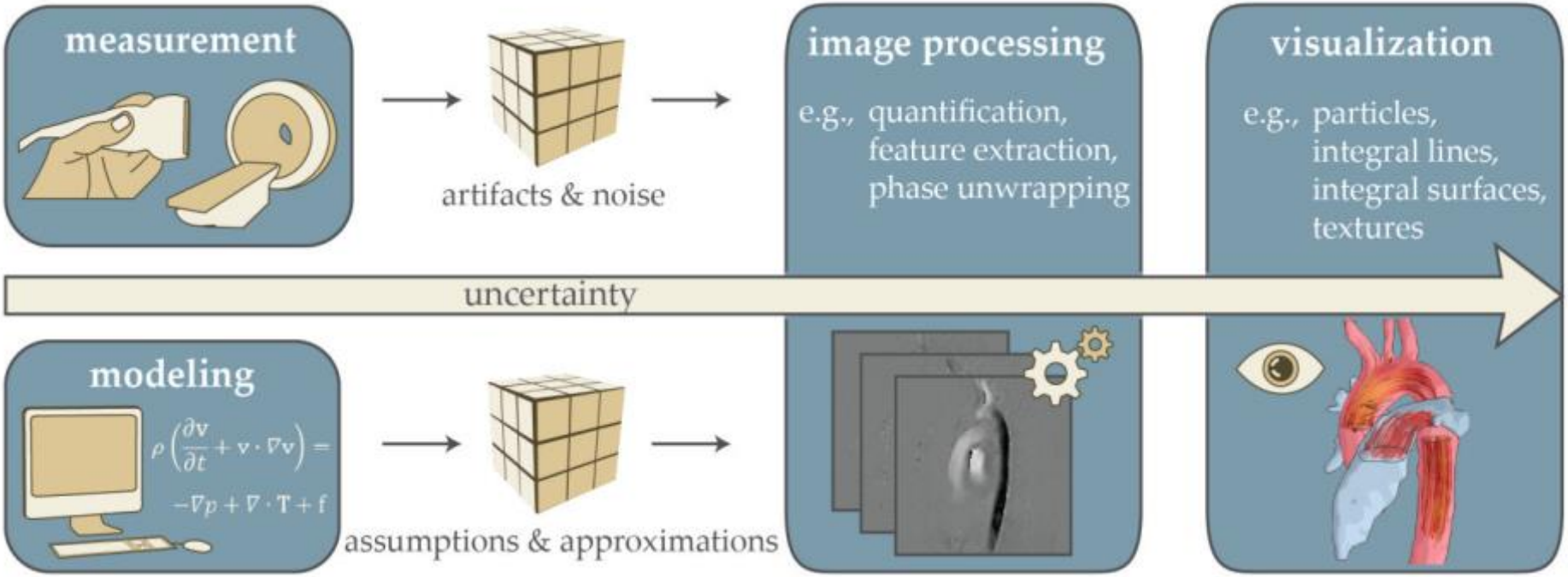

[Van Pelt et al., 2013]

Why do we need complex arterial flows visualizations?

Debakey et al. [1985] showed that the localization of vascular diseases at arterial branches and bends could be **explained by the presence of complex blood flow patterns** at those sites.

Knowledge of accurate blood flow patterns!

Methods of **data reductions are needed** in order to:

- Reduce the complexity of blood flow
- Characterize blood flow dynamics and allow quantitative assessment and comparisons
- Quantify hemodynamic disturbances and ease the clinical interpretation of disturbed flow
- . . .

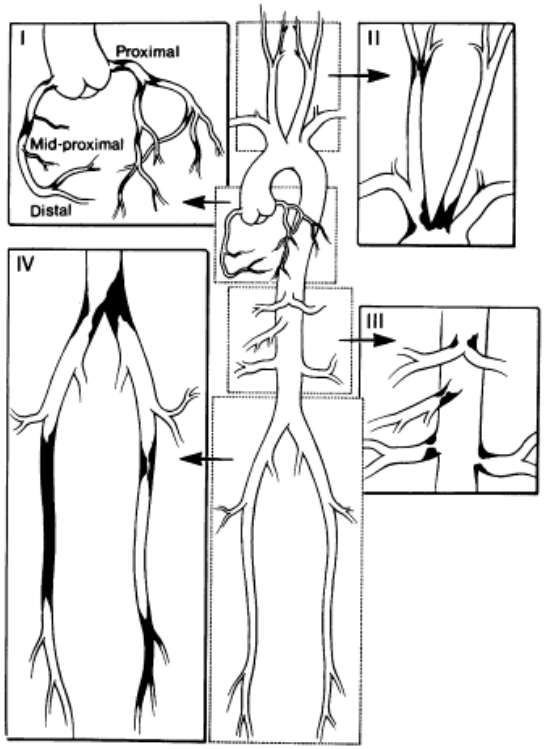

[Debakey et al., 1985]

Atherosclerosis

- Atherosclerosis is a progressive **local thickening** of arteries characterized by lipid deposits in the wall
- **Focal distribution: key role of hemodynamics**

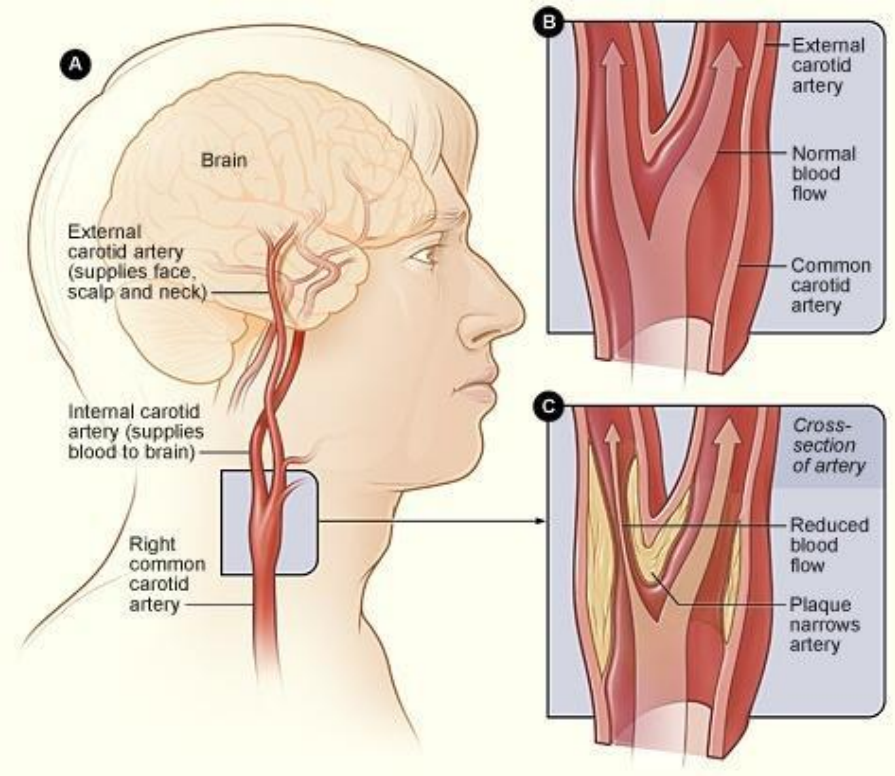

Atherosclerosis

Focal Disease

Bends - Branches - Bifurcations

↓

"Disturbed" Blood Flow

↓

Endothelial Flow-Mediated

Response

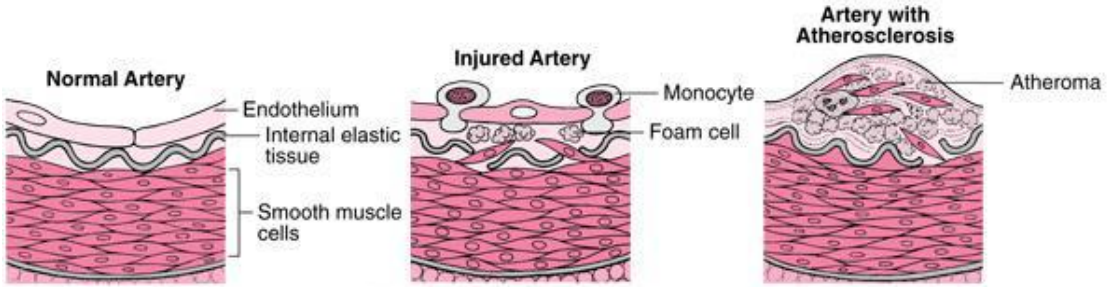

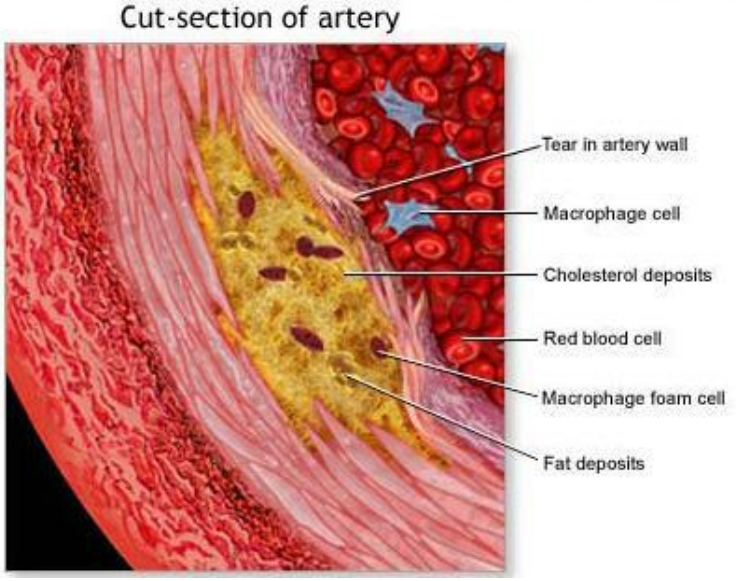

Atherosclerosis

Evidences suggest that initiation and progression of atherosclerotic disease is influenced by **"disturbed flow"**.

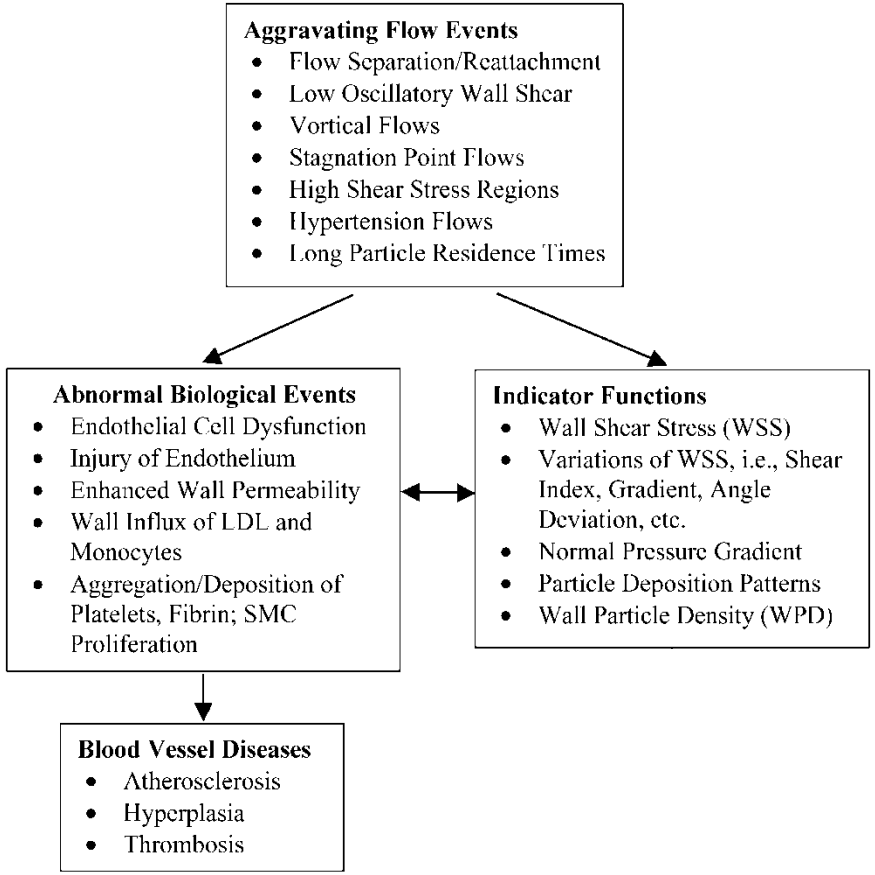

Hemodynamic factors

The role played by **haemodynamic forces acting on the vessel wall** is fundamental in maintaining the normal functioning of the circulatory system, because arteries **adapt to long term variations** in these forces. That is, arteries attempt to re-establish a physiological condition by:

- dilating and subsequently **remodelling** to a larger diameter in the presence of **increased** force magnitude
- remodelling to a smaller diameter, or thickening the intimal layer, in the presence of decreased force magnitude.

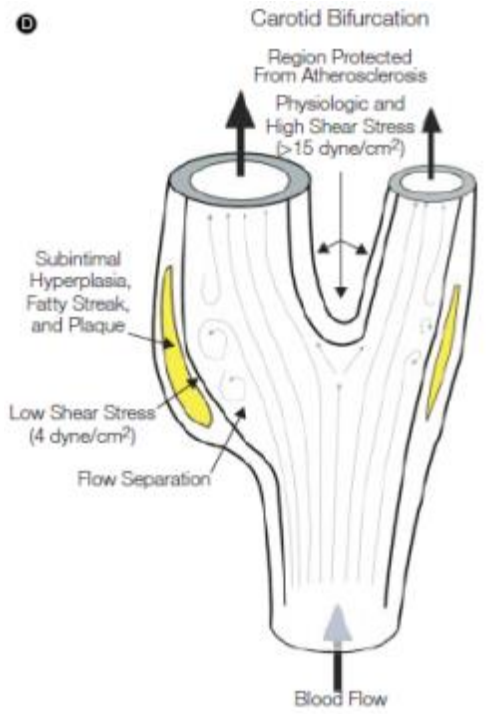

[Malek et al., 1999]

Wall Shear Stress - WSS

- The Wall Shear Stress (WSS), τ_w, is given by:

$$\tau_w = \mu \left(\frac{\partial u}{\partial y}\right)_{y=0}$$

Where μ is the dynamic viscosity, u is the velocity parallell to the wall and y is the distance to the wall.

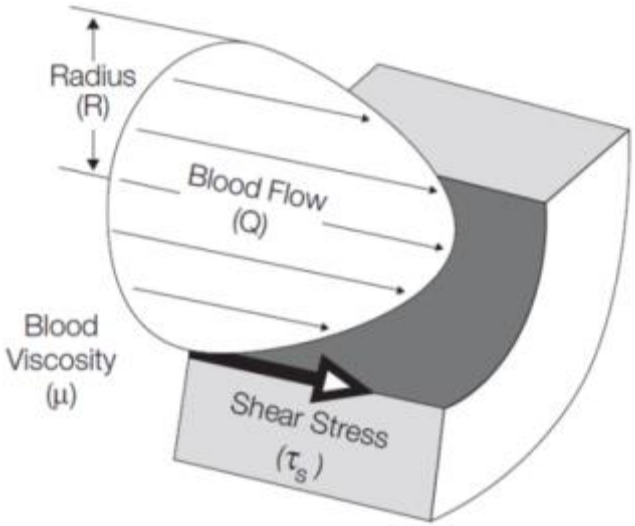

- Low and oscillating WSS has been proposed as a localizing factor of the development of atherosclerosis.

WSS on Endothelial Cells (ECs)

WSS can **change the morphology and orientation** of the endothelial cell layer: endothelial cells subjected to a laminar flow with elevated levels of WSS **tend to elongate and align** in the direction of flow, whereas in areas of disturbed flow endothelial cells experience low or oscillatory WSS and they look more polygonal **without a clear orientation**, with a lack of organization of the cytoskeleton and intercellular junctional proteins.

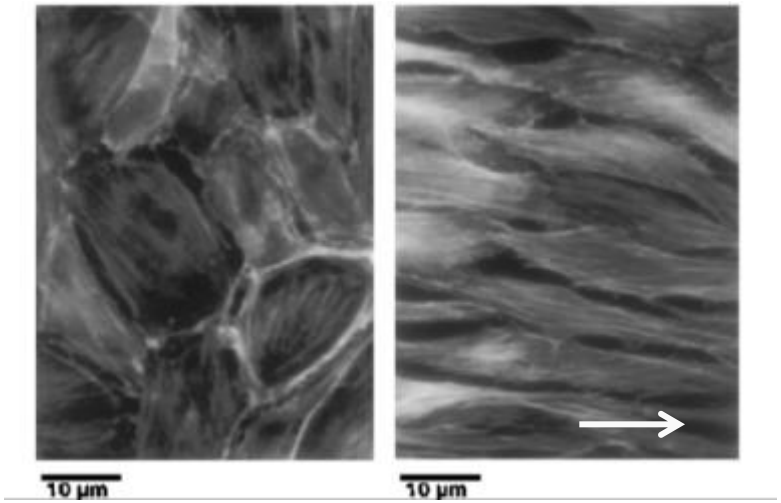

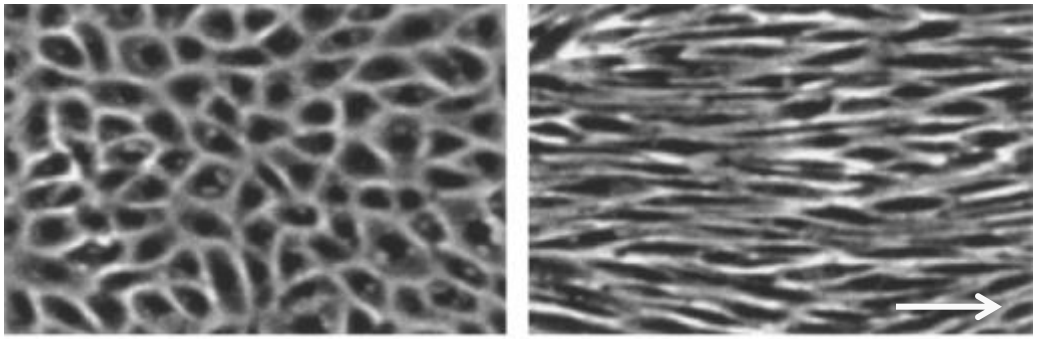

Left: F-actin organization in bovine aortic ECs before and after the application of a steady shear stress. Note extensive F-actin remodeling.
Right: Bovine aortic ECs before flow and after. The cells elongate and align in the direction of flow. [Barakat, 2013]

WSS on Endothelial Cells (ECs)

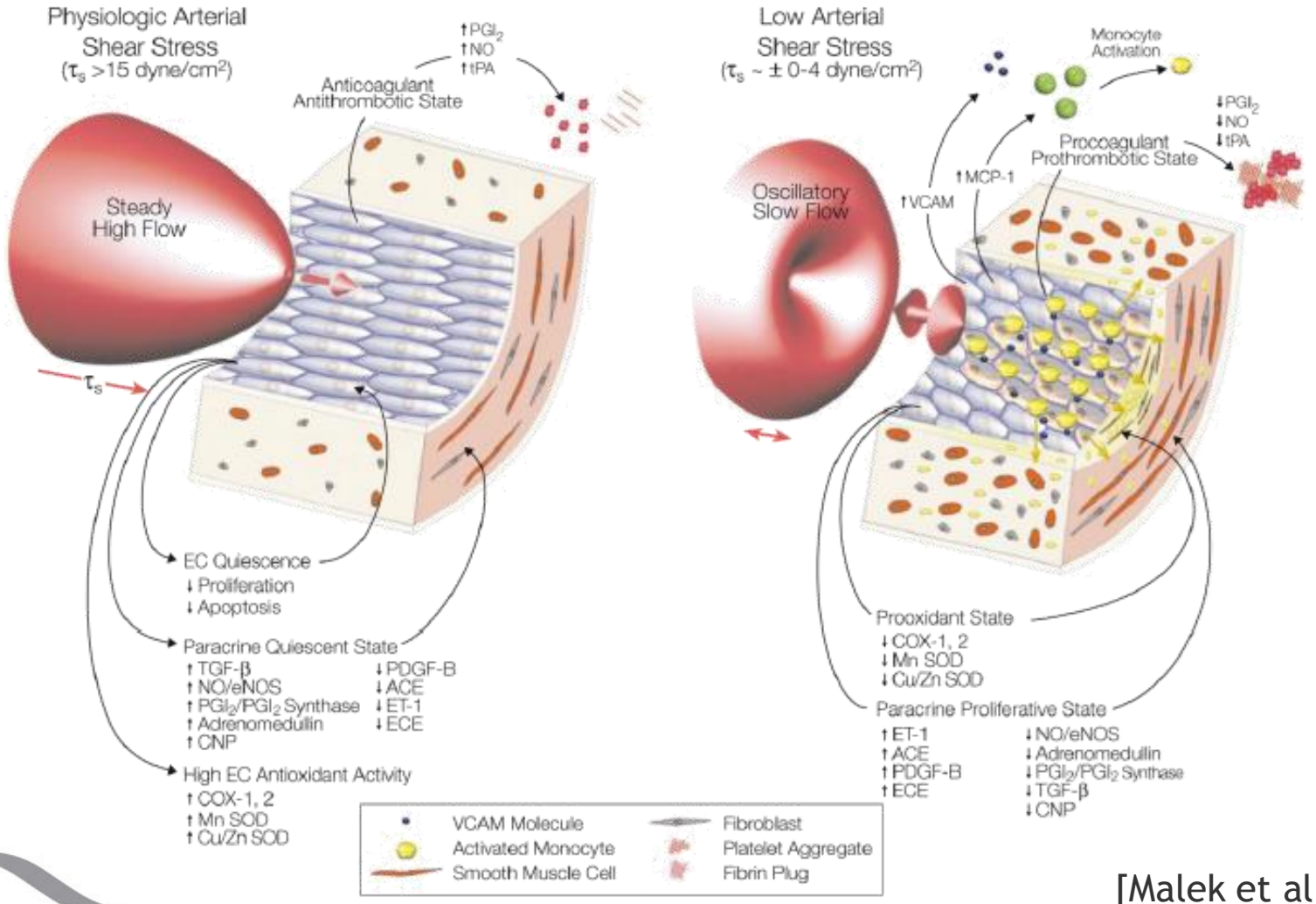

[Malek et al., 1999]

Tool for WSS descriptors: CFD

Imaging + Computational Fluid Dynamics (CFD): reconstruction of complex WSS patterns with a high spatial and temporal resolution.

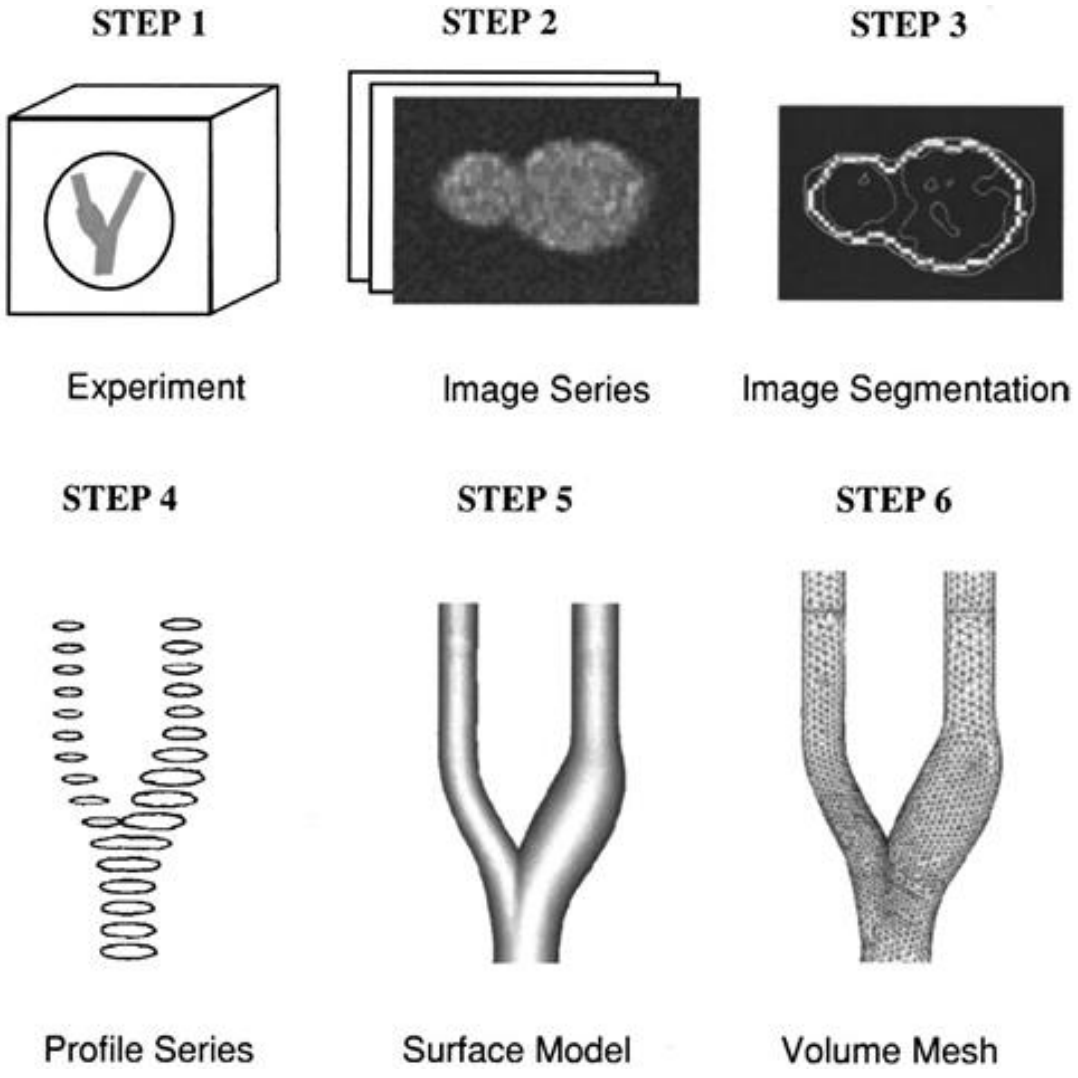

[Steinman 2002]

WSS Descriptors: Time Averaged WSS

- Time-Averaged Wall Shear Stress (TAWSS) can be calculated by **integrating each nodal WSS vector magnitude** at the wall over the cardiac cycle.
- Low TAWSS values (lower than 0.4 Pa) are known to stimulate a **proatherogenic endothelial phenotype**
- Moderate (greater than 1.5 Pa) TAWSS values induces quiescence and an **atheroprotective** gene expression profile.
- High TAWSS values (greater than 10-15 Pa, relevant from 25-45 Pa) can lead to **endothelial trauma**.

$$TAWSS = \frac{1}{T}\int_0^T \left|\mathbf{WSS}(\mathbf{s}, t)\right| \cdot dt$$

[Malek et al., 1999]

WSS Descriptors: Oscillatory Shear Index

- Oscillatory Shear Index (OSI) is used to identify regions on the vessel wall subjected to **highly oscillating WSS directions during the cardiac cycle**. These regions are usually associated with bifurcating flows and flow patterns strictly related to atherosclerotic plaque formation and fibrointimal hyperplasia.
- Low OSI values occur where flow disruption is minimal
- High OSI values (with a maximum of 0.5) highlight sites where the **instantaneous WSS deviates from the main flow direction in a large fraction of the cardiac cycle**, inducing perturbed endothelial alignment.

$$OSI = 0.5 \left[1 - \left(\frac{\left| \int_0^T \mathbf{WSS}(\mathbf{s},t) \cdot dt \right|}{\int_0^T \left| \mathbf{WSS}(\mathbf{s},t) \right| \cdot dt} \right) \right] \qquad 0 \le OSI \le 0.5$$

[Ku et al., 1985]

WSS Descriptors: Relative Residence Time

- Relative Residence Time (RRT) is **inversely proportional to the magnitude of the time-averaged WSS vector** (i.e., the term in the numerator of the OSI formula).
- **Recommended as a robust single descriptor** of "low and oscillatory" shear [Lee et al., 2009].

$$RRT = \frac{1}{(1-2\cdot OSI)\cdot TAWSS} = \frac{T}{\left|\int_0^T \mathbf{WSS}(\mathbf{s},t)\cdot dt\right|}$$

[Himburg et al., 2004]

WSS Descriptors: Gradient-based descriptors

- WSS spatial gradient (WSSG) is **a marker of endothelial cell tension**. It is calculated from the WSS gradient tensor components parallel and perpendicular to the time-averaged WSS vector (m and n, respectively) [Depaola et al., 1992].

$$\mathrm{WSSG} = \frac{1}{T}\int_0^T \sqrt{\left(\frac{\partial \tau_{w,m}}{\partial m}\right)^2 + \left(\frac{\partial \tau_{w,n}}{\partial n}\right)^2}\, dt$$

- The WSS angle gradient (WSSAG) highlights **regions exposed to large changes in WSS direction**, irrespective of magnitude. This is done by calculating, for each element's node (index j), its direction relative to some reference vector (index i, e.g. that at the element's centroid) [Longest et al., 2000].

$$\mathrm{WSSAG} = \frac{1}{T}\int_0^T \left| \frac{1}{A_i}\int\int \nabla \phi_j dA_i \right| dt \;,\; \phi_j = \cos^{-1}\left(\frac{\boldsymbol{\tau}_{w,i}\cdot\boldsymbol{\tau}_{w,j}}{|\boldsymbol{\tau}_{w,i}|\cdot|\boldsymbol{\tau}_{w,j}|}\right)$$

- WSS temporal gradient is the **maximum absolute rate of change in WSS magnitude** over the cardiac cycle.

$$\mathrm{WSST} = \max\left(\left|\frac{\partial|\boldsymbol{\tau}_w|}{\partial t}\right|\right)$$

WSS Descriptors: Harmonic-based descriptors

The harmonic content of the WSS waveforms can be a possible metric of disturbed flow. This statement is enforced by results revealing that **endothelial cells sense and respond to the frequency of the WSS profiles**.

- The time varying WSS magnitude at each node can be Fourier-decomposed, and the dominant harmonic (DH) is defined as the **harmonic with the highest amplitude** [Himburg & Friedman, 2006].

$$\mathrm{DH} = \max(F_w(n\omega_0)),\ F_w \equiv FFT(|\boldsymbol{\tau}_w|),\ \omega_0 = 2\pi/T$$

- The harmonic index (HI) is defined as **the relative fraction of the harmonic amplitude spectrum arising from the pulsatile flow components** [Gelfand et al., 2006].

$$\mathrm{HI} = \sum_{n=1}^{\infty} F_w(n\omega_0) \Big/ \sum_{n=0}^{\infty} F_w(n\omega_0)$$

A matter of information…

The WSS-descriptors **provide essentially the same information** about disturbed flow and many of them can be considered **redundant**!

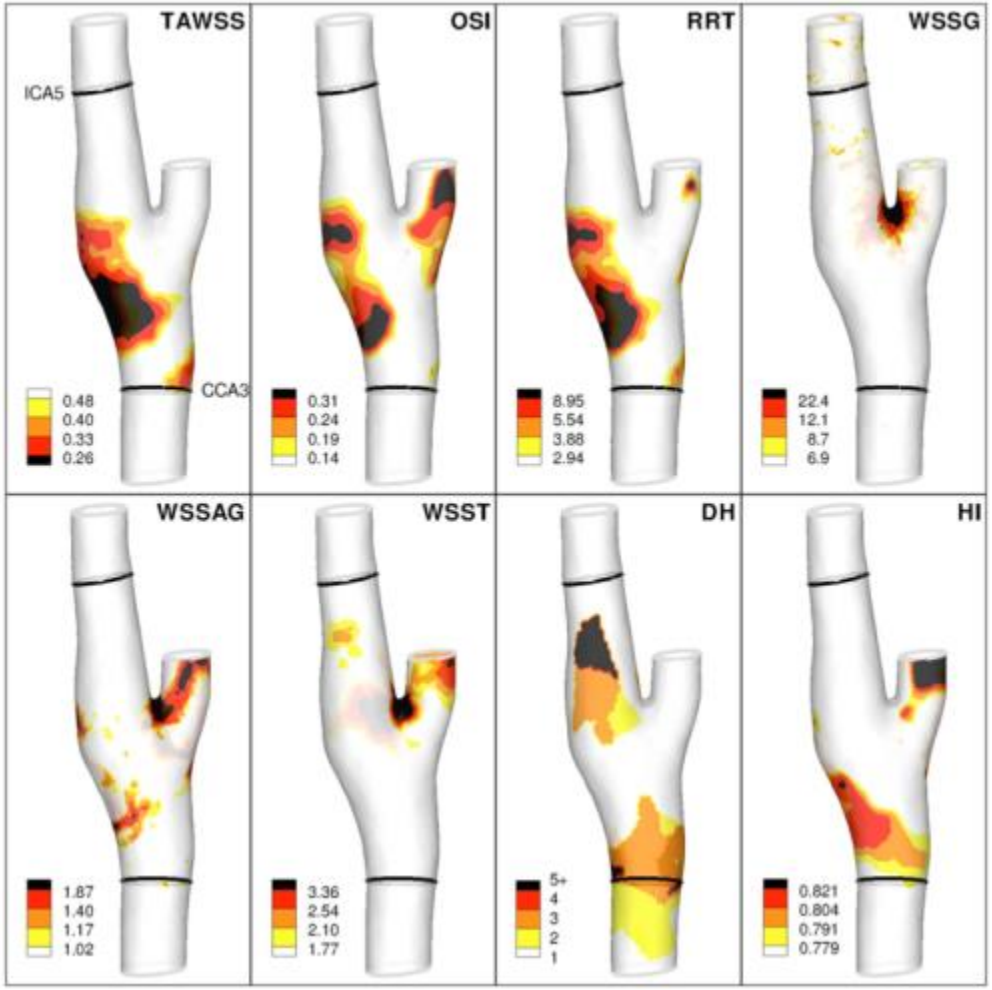

[Lee et al., 2009]

And the bulk flow?

The need for a reduction of the complexity of highly four-dimensional blood flow fields, aimed at identifying **hemodynamic actors involved in the onset of vascular pathologies**, was driven by **histological observations on samples of the vessel wall.**

Disturbed flow within arterial vasculature has been primarily quantified in terms of **WSS-based metrics.**

This strategy was applied notwithstanding **arterial hemodynamics is an intricate process** that involves interaction, reconnection, and continuous re-organization of structures in the fluid!

The investigation of the role played by the bulk flow in the development of the arterial disease needs **robust quantitative descriptors with the ability of operating a reduction of the complexity of highly 4D flow fields.**

[Morbiducci et al., 2010]

Eulerian *vs.* Lagrangian

Lagrangian	Eulerian
+ Visualizations + Three dimensionality/ Four dimensionality (i.e., space and time) + Highlight of the recirculation zones + Characterization of unsteady flow patterns + More immediate understanding of the fluid motion + Path dependent quantities + Dynamical path history + Division of particles into groups regardless of position - Convectiveness: less control over the zone of investigation - Computational cost - Timing: it is difficult to picture the flow at a specific time instant	+ Simplicity + Picture of the entire flow + Timing + Real time analysis + Its immediateness is attractive for clinicians

[Gallo et al., 2013]

How to reduce flow complexity?

Helicity influences evolution and stability of both turbulent and laminar flows [Moffatt and Tsinober, 1992]. Helical flow patterns in arteries **originate to limit flow instabilities** potentially leading to atherogenesis/atherosclerosis.

An arrangement of the bulk flow in complex helical/vortical patterns might **play a role in the tuning of the cells mechano-transduction pathways**, due to the **relationship between flow patterns and transport phenomena** affecting blood-vessel wall interaction, like residence time of atherogenic particles.

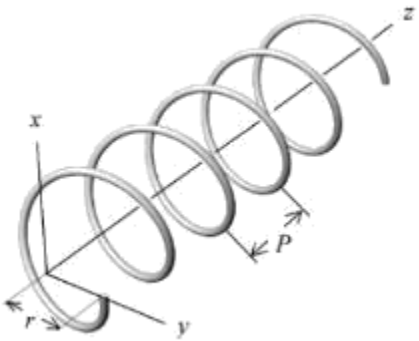

[Morbiducci et al., 2007, 2009, 2010, 2011: Gallo et al., 2012]

Helicity – Lagrangian Metric

Starting from the definition of helicity density

$$H_k(\mathbf{s};\, t) = \mathbf{V} \cdot (\nabla \times \mathbf{V}) = \mathbf{V}(\mathbf{s};\, t) \cdot \boldsymbol{\omega}(\mathbf{s};\, t)$$

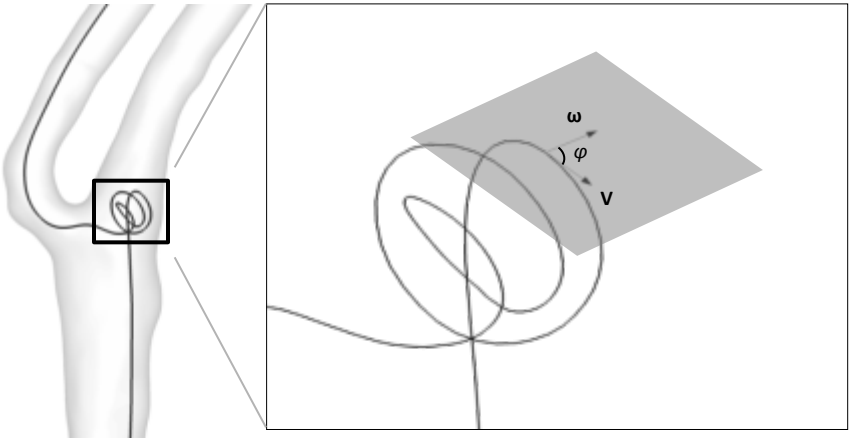

The Local Normalized Helicity (LNH) is defined as:

$$\mathrm{LNH}(\mathbf{s};t) = \frac{\mathbf{V}(\mathbf{s};t) \cdot \boldsymbol{\omega}(\mathbf{s};t)}{|\mathbf{V}(\mathbf{s};t)|\,|\boldsymbol{\omega}(\mathbf{s};t)|} = \cos\varphi(\mathbf{s};t)$$

The helical structure of blood flow was measured calculating the Helical Flow Index (HFI) over the trajectories of the Np particles present within the domain:

$$hfi_k = \frac{1}{(T_k^{end} - T_k^{start})} \int_{T_k^{start}}^{T_k^{end}} |\mathrm{LNH}_k(\varsigma)|\, d\varsigma \qquad \mathrm{HFI} = \frac{1}{N_p} \sum_{k=1}^{N_p} hfi_k \qquad 0 \le \mathrm{HFI} \le 1$$

where Np is the number of points j (j = 1:Np) along the k-th trajectory.

[Grigioni et al. 2005, Morbiducci et al. 2007]

Helicity - Eulerian Metrics

Descriptor	Definition	Description
h_1	$\frac{1}{V}\int_{T_i}\int_{V_i} H_k \, dV \, dt$	Integral measure of helicity, accounting for changes in sign of H_k.
h_2	$\frac{1}{V}\int_{T_i}\int_{V_i} \lvert H_k \rvert \, dV \, dt$	Integral measure of the absolute value of H_k: total amount of helicity in the fluid domain.
h_3	$\frac{h1}{h2}$	Its value equals -1 (+1) when only left-handed (right-handed) helical structures are present in the domain and it equals 0 in case of reflectional symmetry.
h_4	$\lvert h3 \rvert = \frac{\lvert h1 \rvert}{h2}$	As for h3, but neglecting what is the major direction of rotation.
h_5	$\frac{\int_{T_i}\int_{V_{i\,d}} dV_d \, dt}{\int_{T_i}\int_{V_{i\,m}} dV_m \, dt}$	Ratio between the volumes of the fluid domain occupied by helical rotating structures. The volume occupied by the dominant direction (V_d) of rotation is the numerator,the volume occupied by the minor direction of rotation (V_m) being the denominator
h_6	$\frac{\frac{1}{V_d}\int_{T_i}\int_{V_{i\,d}} H_{k\,d} \, dV_d \, dt}{\frac{1}{V_m}\int_{T_i}\int_{V_{i\,m}} H_{k\,m} \, dV_m \, dt}$	Ratio between the mean volumetric helicity values over the volume occupied by the dominant and the minor direction of rotation

[Gallo et al., 2012]

Hemodynamic Descriptors

Examples of *in silico* and *in vivo* applications

Influence of Blood Rheology

Background

- CFD modeling requires assumptions
- Blood widely assumed as a **Newtonian fluid**

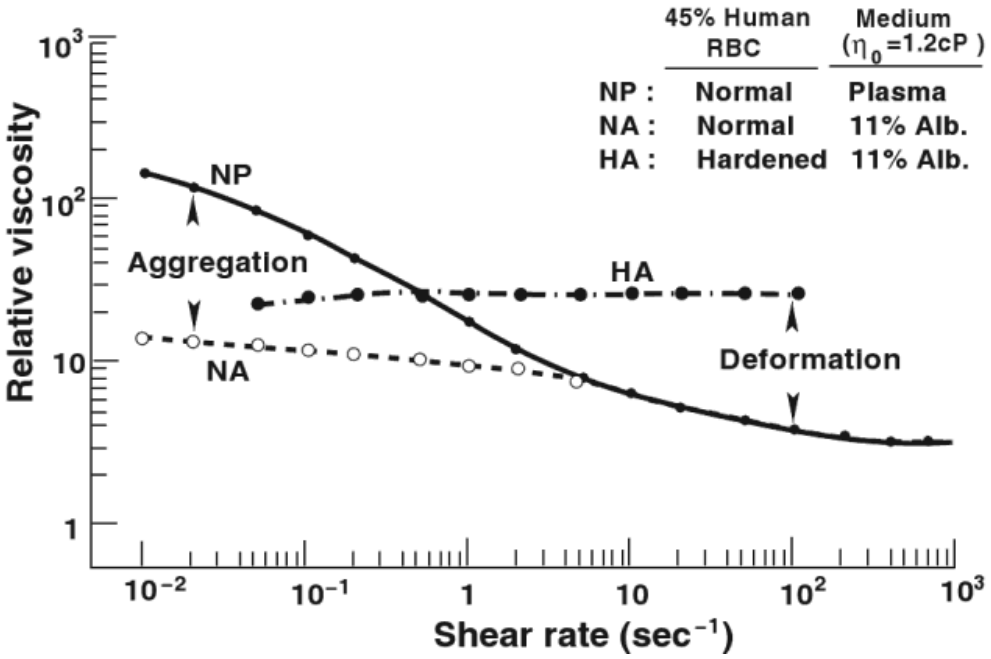

Aim

Evaluate the influence of blood rheological properties on **WSS** and **bulk flow**

[Morbiducci et al., 2011]

Computational Models

- Image-based 3D models of carotid bifurcation from CT images
- Discretisation in 1.4·106 (A), 1.2·106 (B) cells (Gambit, ANSYS)
- CFD code based on finite volume method (Fluent 6.3.2, ANSYS)
- Unsteady flow conditions and rigid walls with no-slip conditions
- Fixed flow rate distribution of 60/40 at ICA and ECA outlet sections

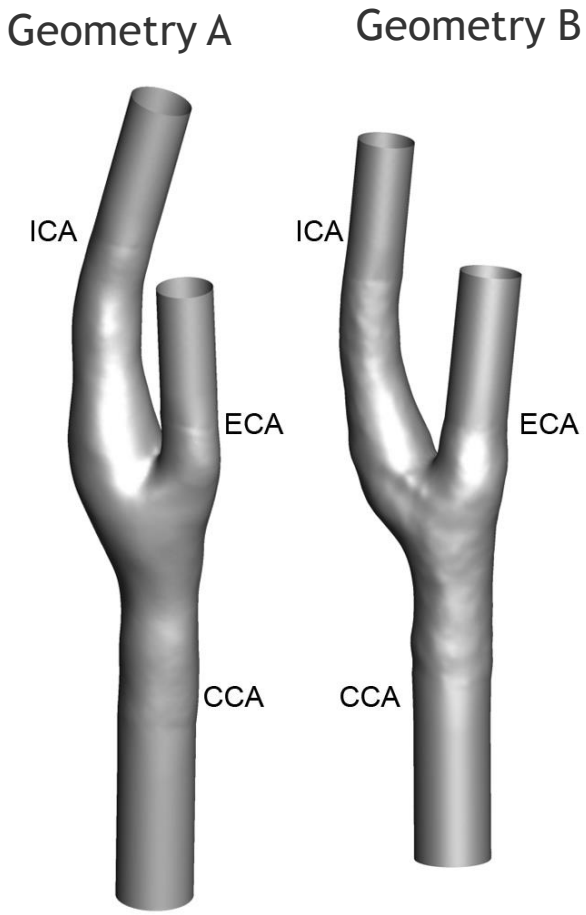

CCA – common carotid artery

ECA – external carotid artery

ICA – internal carotid artery

Rheological Models

Blood assumed:
- **isotropic**
- **incompressible** (ρ=1060 kg/m^3)
- **Newtonian model** with μ = **3.5 cP** (reference model, Ht = 43%)

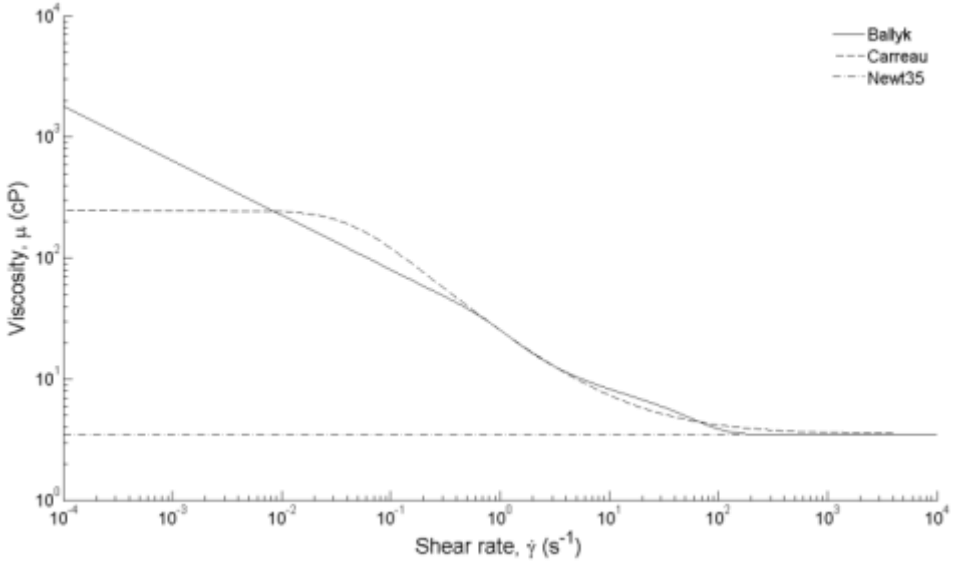

Non-Newtonian models:

- **Ballyk model**

$$\mu(\dot{\gamma}) = \lambda(\dot{\gamma})\dot{\gamma}^{n(\dot{\gamma})-1}$$

- **Carreau model**

$$\mu(\dot{\gamma}) = \mu_\infty + (\mu_0 - \mu_\infty)\left[1+(\lambda\dot{\gamma})^2\right]^{n-\frac{1}{2}}$$

viscosity function (μ) dependent on shear rate
(μ_∞ = 3.5 cP, models tuned according to mean Ht = 43%)

Rheological Models

Newtonian models with viscosity derived from the Carreau model at characteristic shear rates [Gijsen et al. 1999]:

$$\dot{\gamma}_c = \frac{8V}{3R}$$

Corresponding to the minimum and mean inlet flow rate.

	$\dot{\gamma}_c^{MIN}$ [s^{-1}]	μ_c^{MIN} [cP]	Ht	$\dot{\gamma}_c^{MEAN}$ [s^{-1}]	μ_c^{MEAN} [cP]	Ht
A	79.68	4.14	0.48	122.90	3.96	0.47
B	82.04	4.12	0.48	126.10	3.95	0.47

Results – WSS Descriptors

On regions exposed to low and oscillating WSS, the absolute percentage differences with respect to Newt35 are up to :

A	TAWSS	OSI	RRT
Max % diff. vs. Newt35	12.5%	4.5%	28.0%
Rheological model	μ_C^{MIN}	Ballyk	μ_C^{MEAN}

B	TAWSS	OSI	RRT
Max % diff. vs. Newt35	39.8%	8.0%	14.7%
Rheological model	Ballyk	Ballyk	Carreau

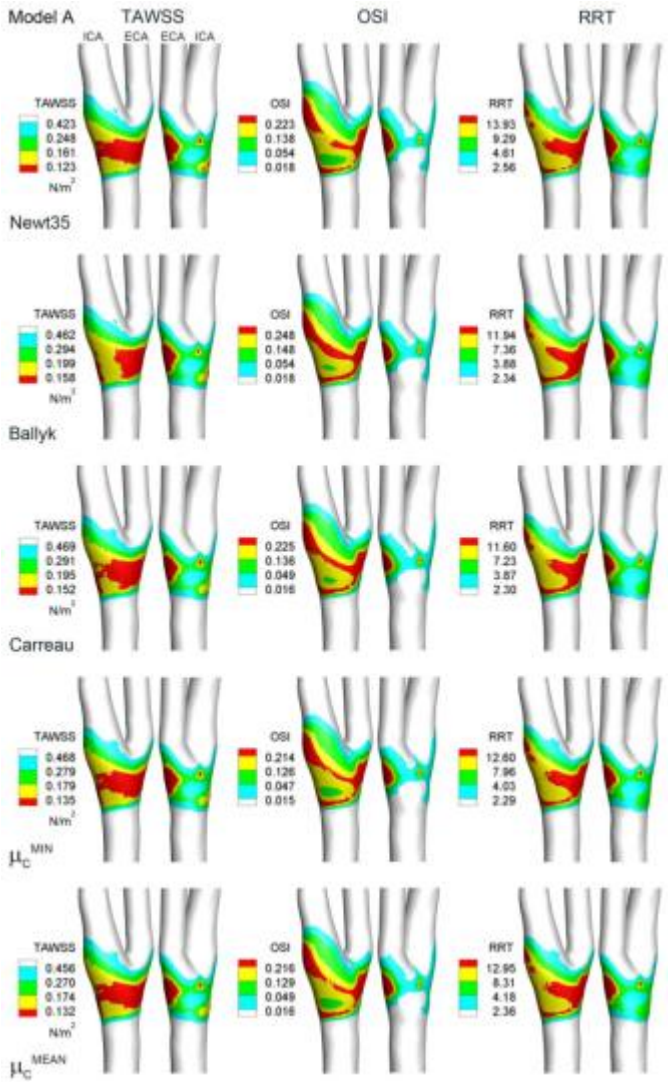

Results - Helical flow

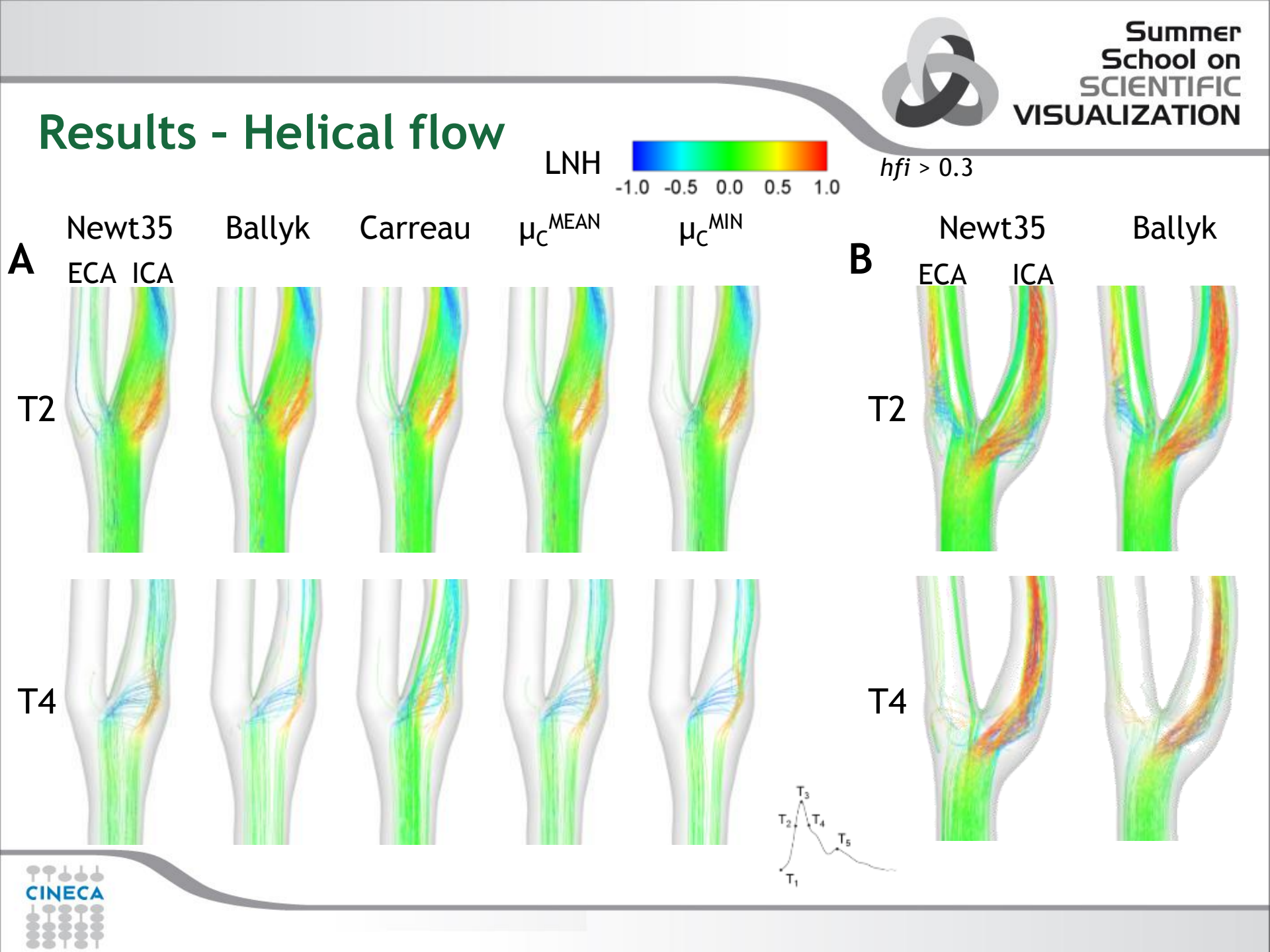

Conclusions

The assumption of **Newtonian behaviour** is **reasonable** in the context of currently available level of uncertainty related to geometric reconstruction (differences in WSS-based parameters of 48% [Thomas et al. 2005]) both for WSS-based parameters and bulk flow descriptors.

Geometric reconstruction has primary influence on physiologically significant indicators.

Influence of Outlet BCs

Computational results are very **sensitive to the type of boundary conditions** (BCs) employed for the model

Since the computational model is studied as isolated from the rest of the arterial tree, **the outlet BC should represent downstream vasculature.**

Aim

A **coupled multiscale** (MS) **model** is proposed to study the influence of outflow BCs on TAWSS, OSI, RRT, HFI.

[Morbiducci et al., 2010]

Computational model

The 3D model is coupled with a 0D lumped parameters *RCR* model

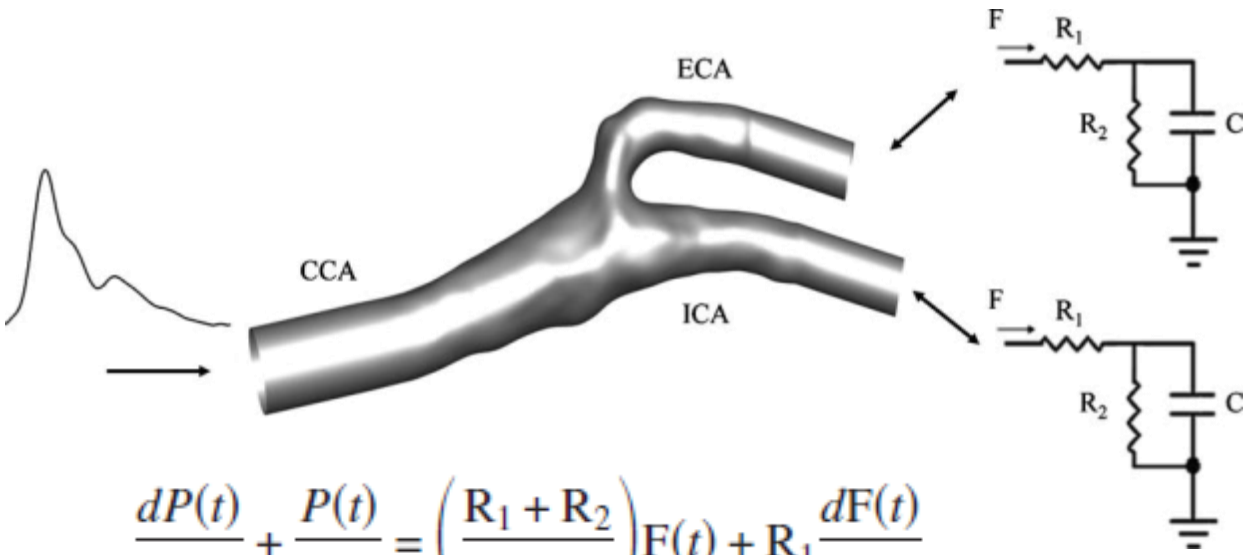

$$\frac{dP(t)}{dt} + \frac{P(t)}{R_2 C} = \left(\frac{R_1 + R_2}{R_2 C}\right) F(t) + R_1 \frac{dF(t)}{dt}$$

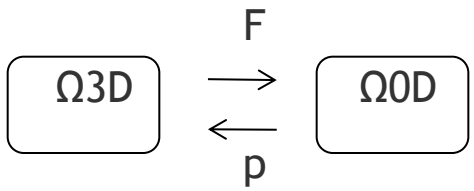

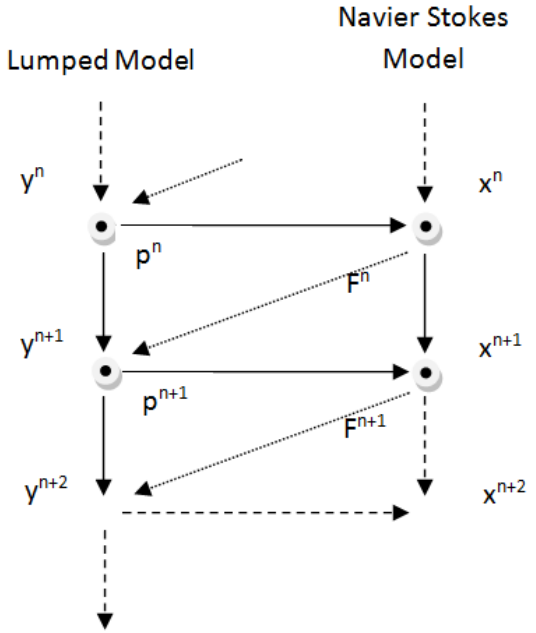

Case studies:

- Multiscale
- ICA/ECA flow division:
  - 50/50
  - 60/40
  - 70/30

Results – WSS Descriptors

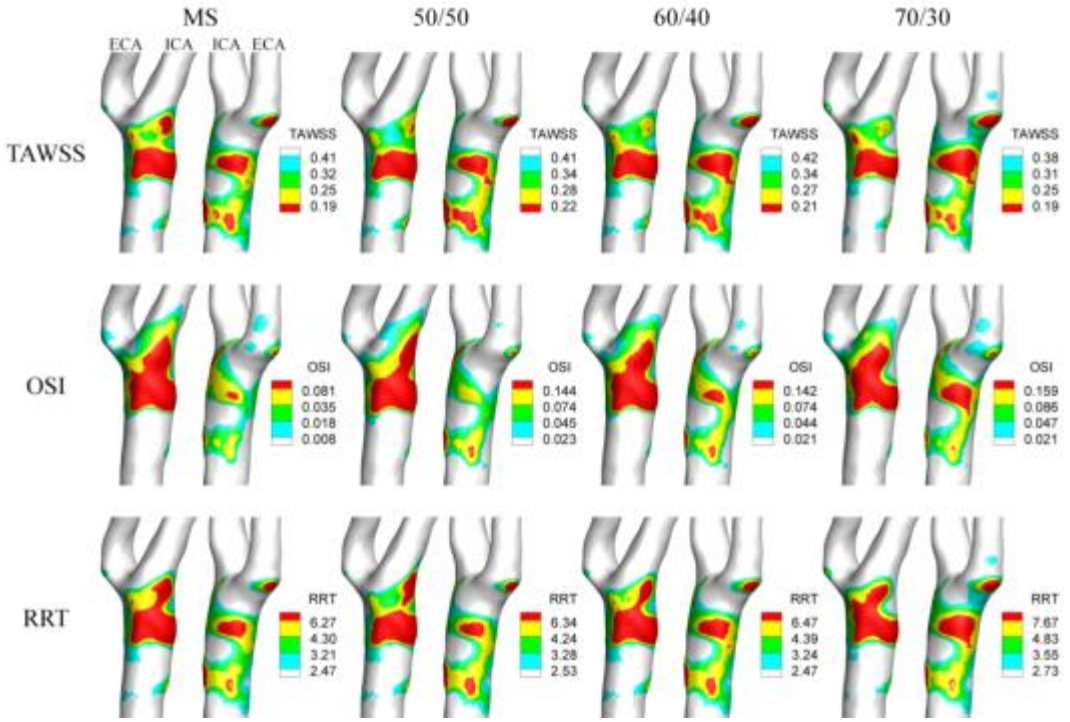

	TAWSS	OSI	RRT
Max % diff. vs. MS	22,9%	37,3%	16,6%
Flow division	50/50	70/30	50/50

Results - Helical flow

The coupled model is characterized by the **most damped dynamics** in term of helical flow.

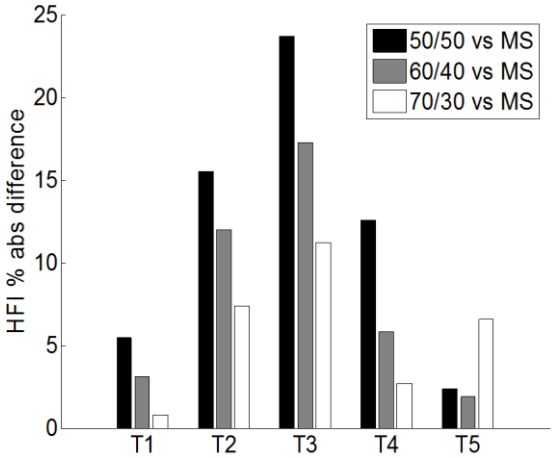

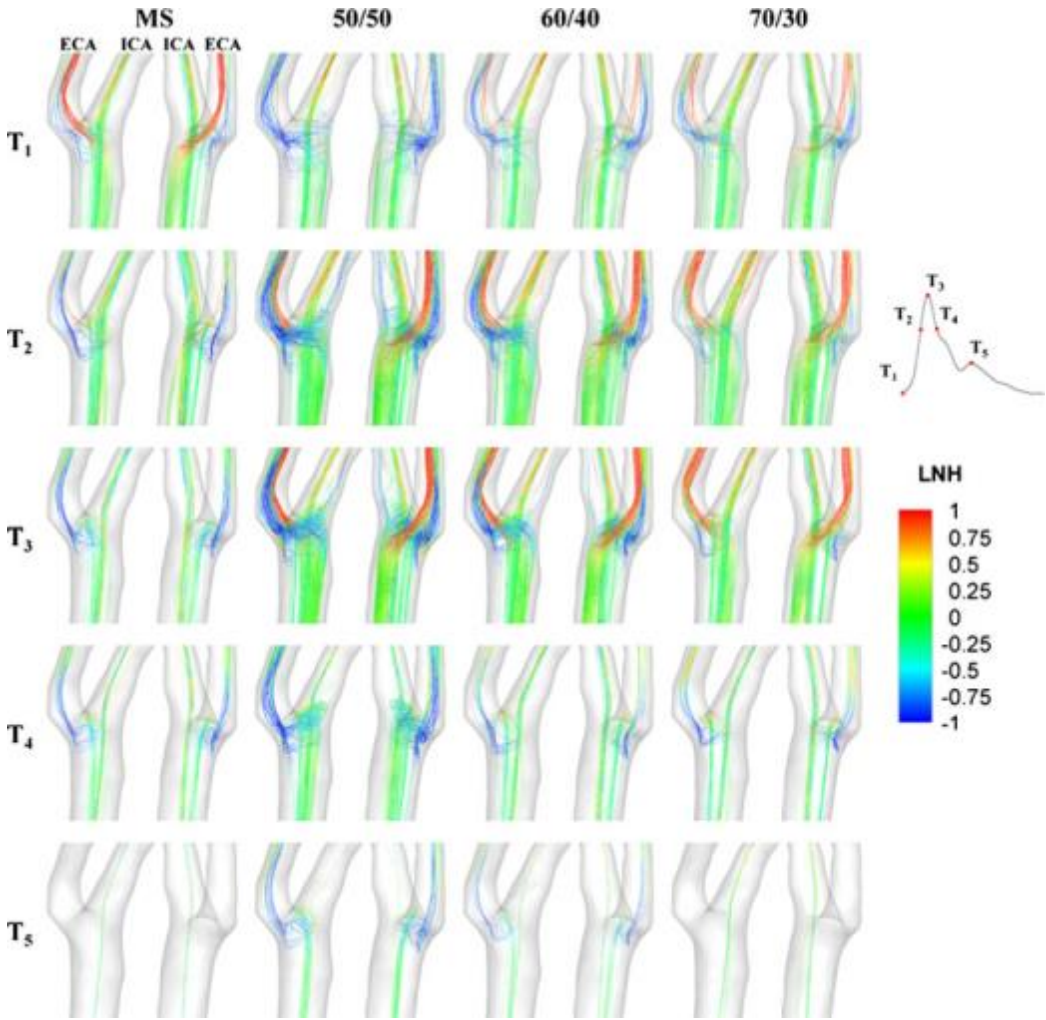

Conclusions

- With the use of a multiscale approach, it is possible to model a **realistic** (physical) downstream BCs for carotid bifurcation
- The coupled simulation **damps WSS oscillations and helical flow dynamics**, **reducing the complexity** of the flow within the bifurcation.
- **Percentage variations observed are greater** than the ones observed varying **blood rheology.**
- The coupling strategy is recommended **when hemodynamics measurements are not available**, **when predicting the outcome** of alternate therapeutic intervention, or to **relate local factors to global factors** in vascular disease.

Relationships among WSS descriptors and helical flow descriptors

CFD models as proof of concept for the **discovery of relationships among measurable quantities** [Harloff et al. 2009; Morbiducci et al. 2011] and **exposure to disturbed shear**

Aim

Demonstration that bulk flow feature analysis offer a practical way to large scale in vivo studies of local risk factors.

[Gallo et al., 2012]

Computational Dataset

Image-based 3D models of carotid bifurcation from black blood MRI

CFD code based on finite element method

Metrics for disturbed shear: fraction of the luminal surface exceeding a objective threshold of TAWSS, OSI and RRT.

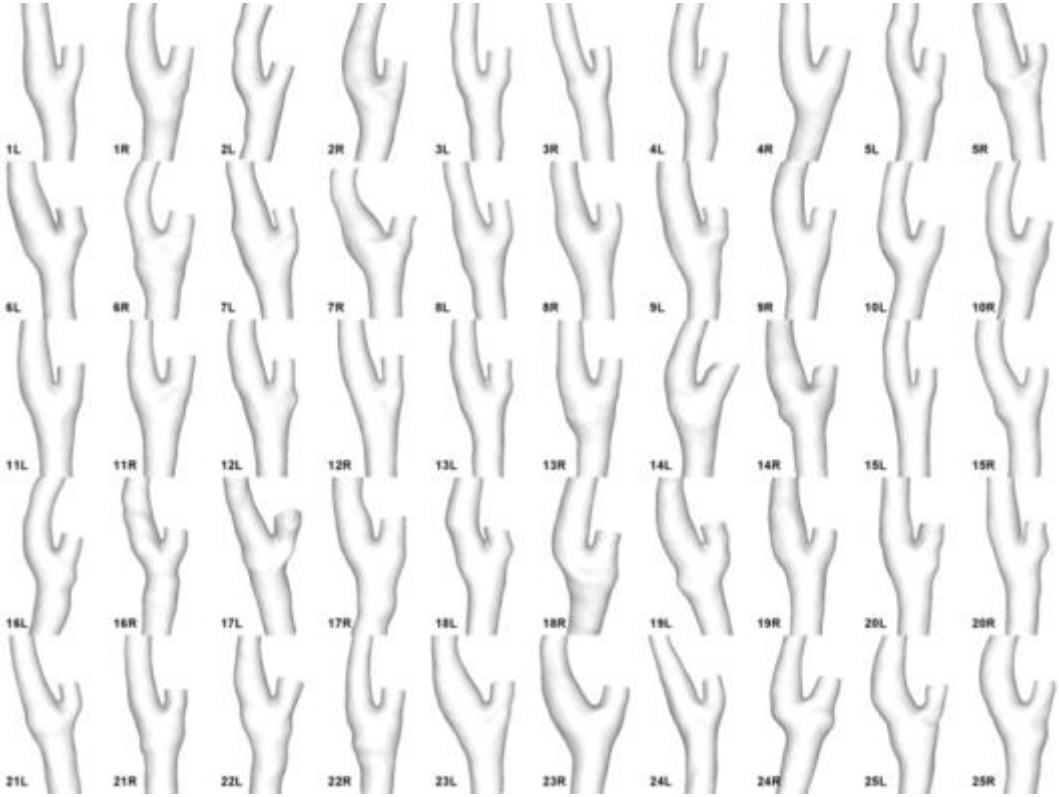

[Lee et al. 2008]

RRT results

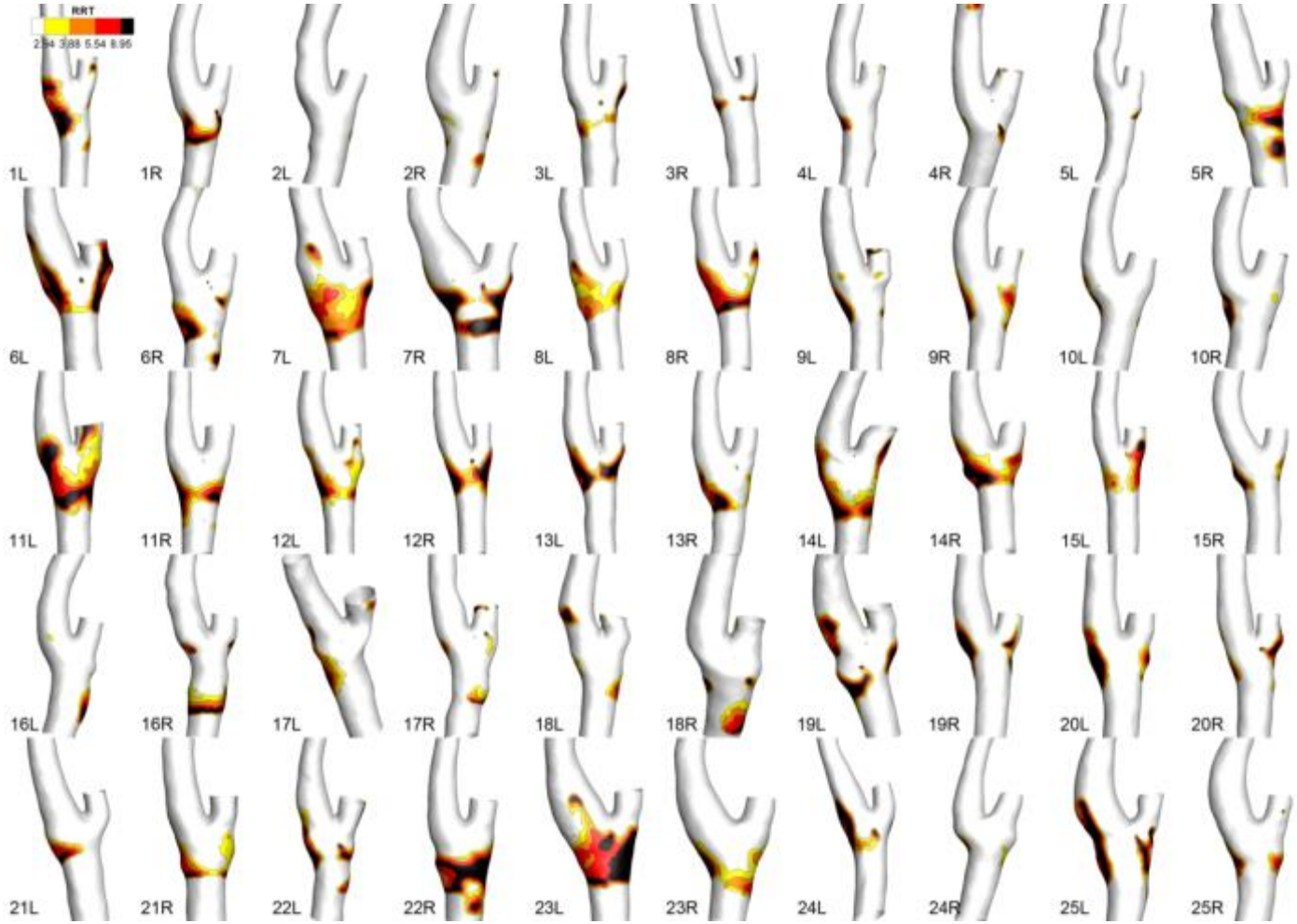
RRT
2.54 3.88 5.54 8.95
1L
1R
2L
2R
3L
3R
4L
4R
5L
5R
6L
6R
7L
7R
8L
8R
9L
9R
10L
10R
11L
11R
12L
12R
13L
13R
14L
14R
15L
15R
16L
16R
17L
17R
18L
18R
19L
19R
20L
20R
21L
21R
22L
22R
23L
23R
24L
24R
25L
25R

LNH visualizations

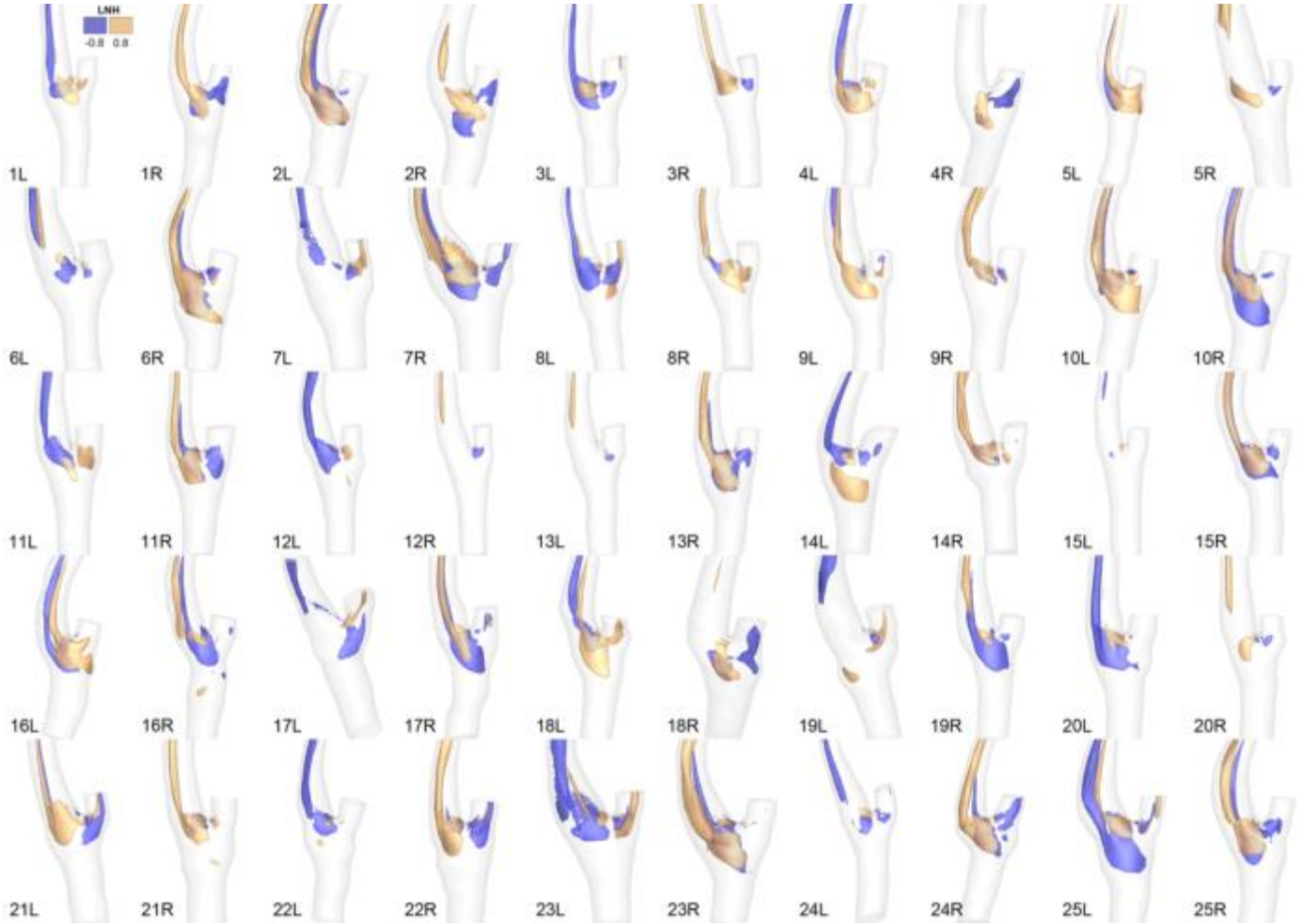

Relationship WSS - helicity

($P<0.0001$)		V_{FULL}	V_1	V_{CCA}	V_{ICA}	$V_{CCA+ICA}$
RRT80	R^2_{adj}	0.576	0.685	0.646	0.396	0.521
	Model	$\{h_2,h_4\}$	$\{h_2\}$	$\{h_2\}$	$\{h_2,h_4\}$	$\{h_2,h_4\}$
RRT90	R^2_{adj}	0.461	0.599	0.547	0.352	0.396
	Model	$\{h_2,h_4\}$	$\{h_2\}$	$\{h_2\}$	$\{h_2,h_4\}$	$\{h_2,h_4\}$

- Surface area (SA) exposed to disturbed shear can be described by:

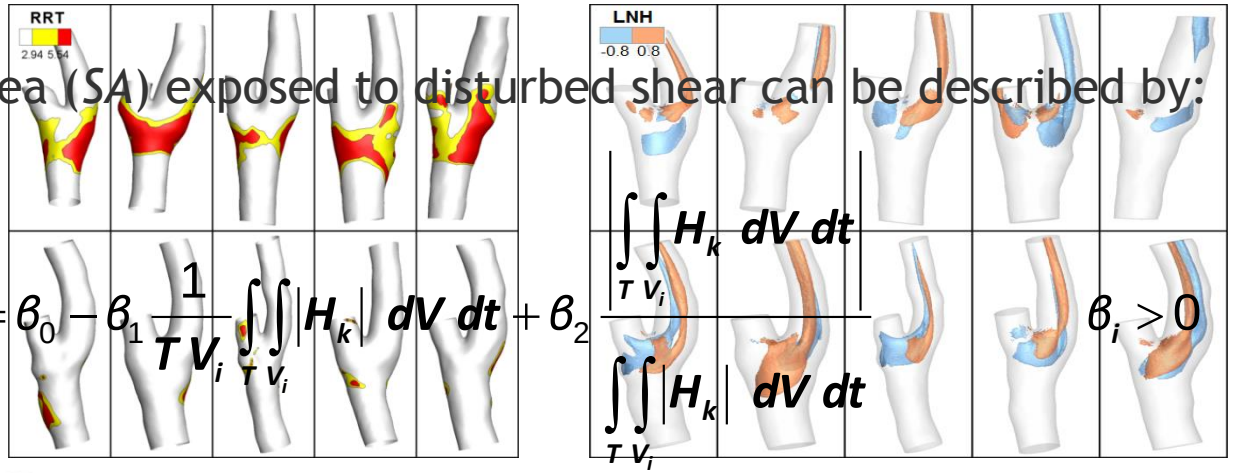

$$SA = \beta_0 - \beta_1 \frac{1}{TV_i} \int_{TV_i} \int \left| H_k \right| \, dV \, dt + \beta_2 \frac{\left| \int_{TV_i} \int H_k \, dV \, dt \right|}{\int_{TV_i} \int \left| H_k \right| \, dV \, dt} \qquad \beta_i > 0$$

Conclusions

- A **high amount of helicity is instrumental in suppressing flow disturbances**; this protective effect can be moderated when one direction of rotation is dominant in the flow field.
- The helicity-based descriptors defined in this section **could be used to classify risk and identify individuals at greater susceptibility for vascular disease** in carotid bifurcation
- Bulk flow feature analysis offer **a practical way to large scale studies of local risk factors** providing **measurable indicators** of potential clinical use.

Summary – carotid bifurcation

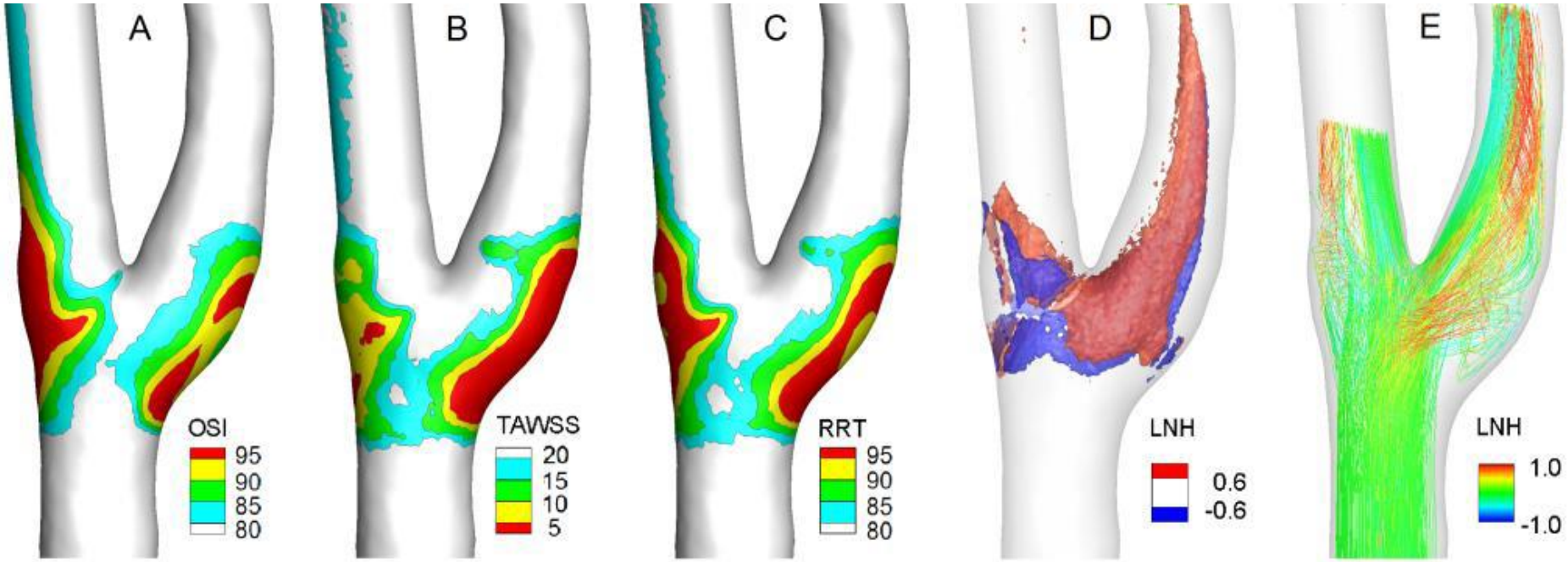

[Gallo et al., 2013]

Coronary artery stenting

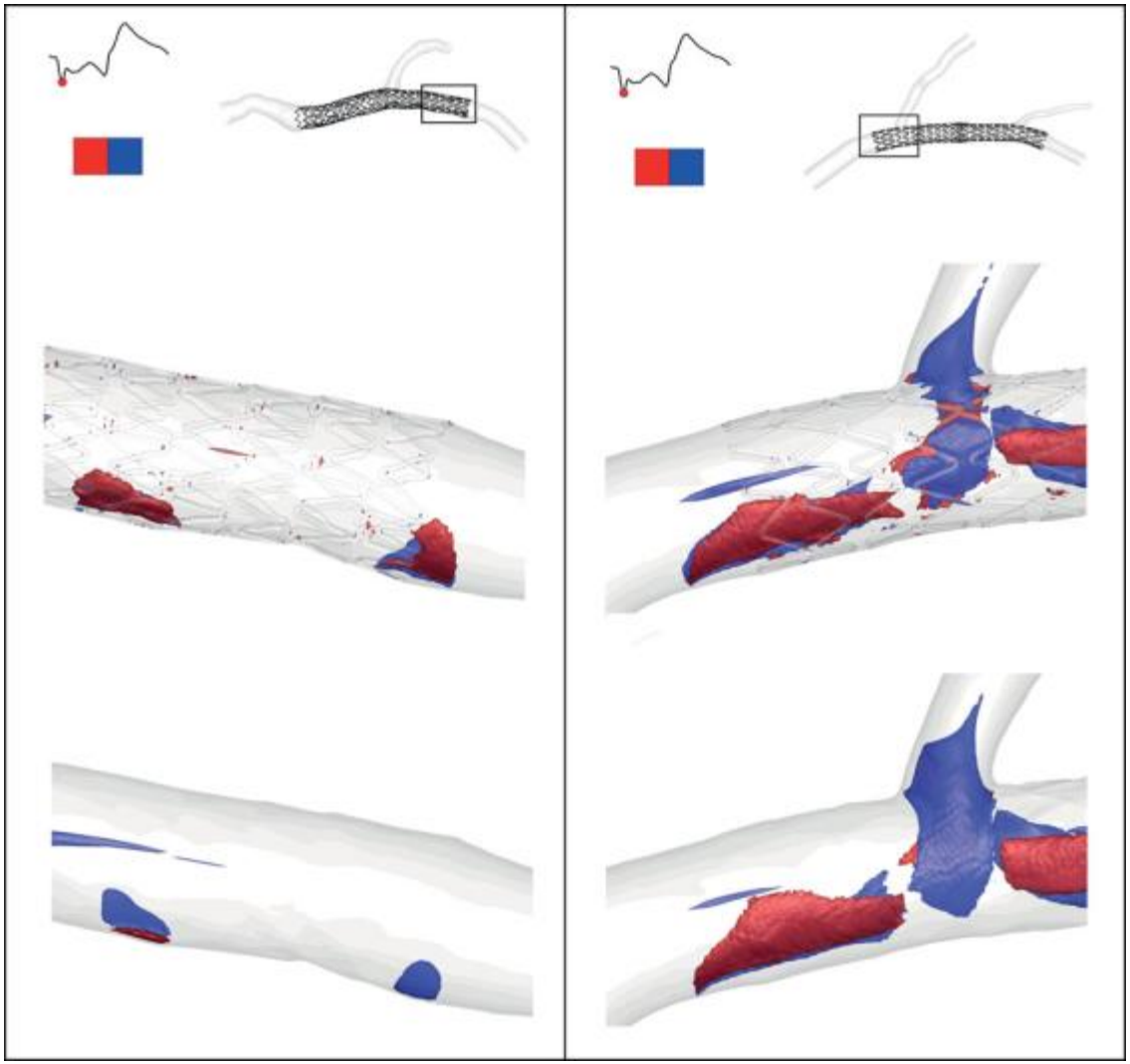

[Chiastra et al., 2013]

Thoracic Aorta

PC-MRI Acquisition

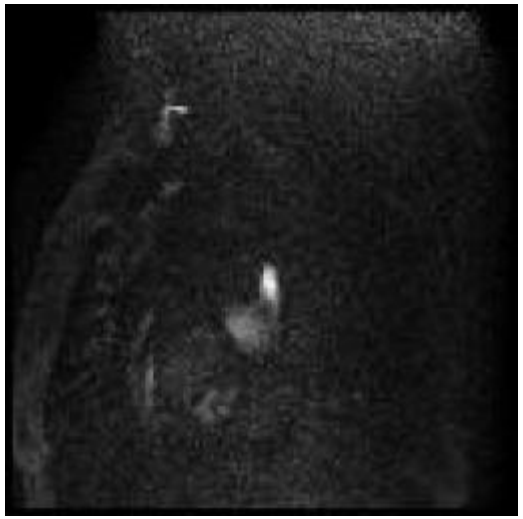

Geometric Model Reconstruction

AAo – ascending aorta
BCA – brachiocephalic artery
LCCA – left common carotid artery
LSA – left subclavian artery
DAo – descending aorta

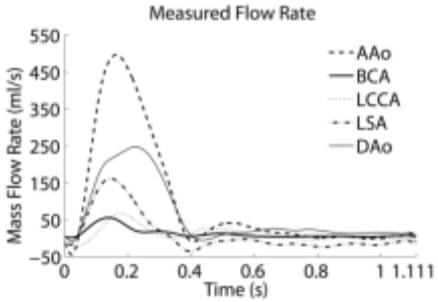

BCs & 4D Velocity Profiles Extraction

- Solver: Fluent 6.3 (ANSYS)
- Newtonian blood rheology model (Ht: 43%, ρ: 1060 kg/m^3, μ : 3.5 cP)
- Rigid walls are assumed

[Gallo et al., 2012]

Outlet BCs strategies

[Gallo et al., 2012]

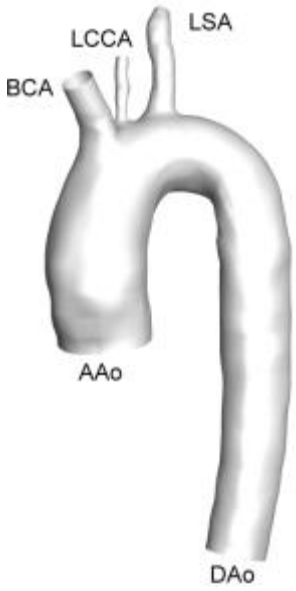

Indicators:
TAWSS, OSI, RRT

MFR: Measured Flow Rate Waveform
SF: Stress-free condition
COR: Constant Outflow Ratio (measured fraction of AAo inlet flow rate)

Outlet Treatment Scheme	BCA	LCCA	LSA	DAo
S1	COR	COR	COR	SF
S2	SF	SF	SF	MFR
S3	SF	SF	SF	SF
S4	COR	COR	SF	MFR
S5	MFR	SF	SF	MFR
S6	MFR	MFR	MFR	SF

4D measured velocity profiles

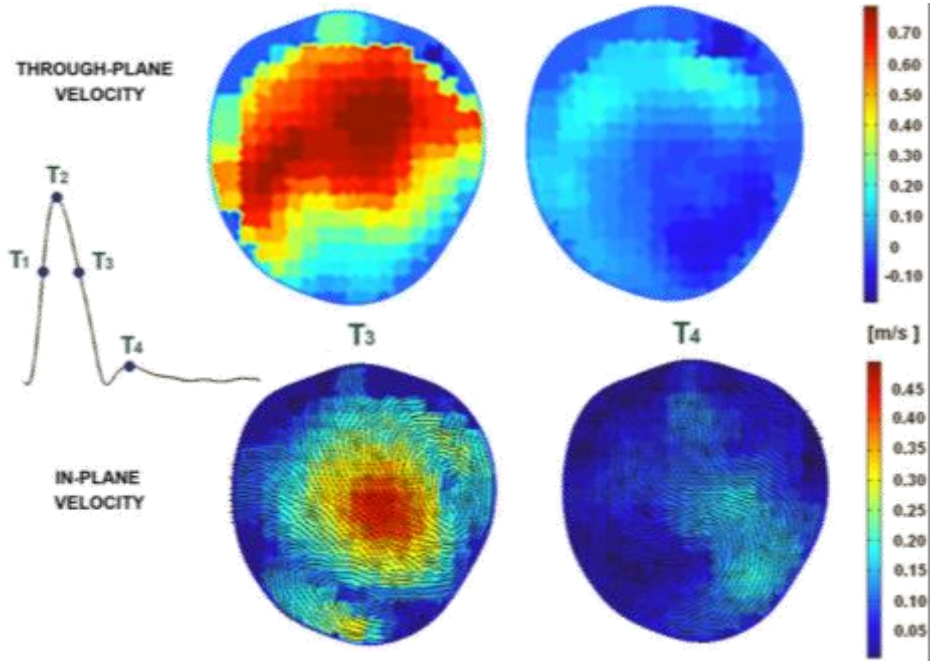

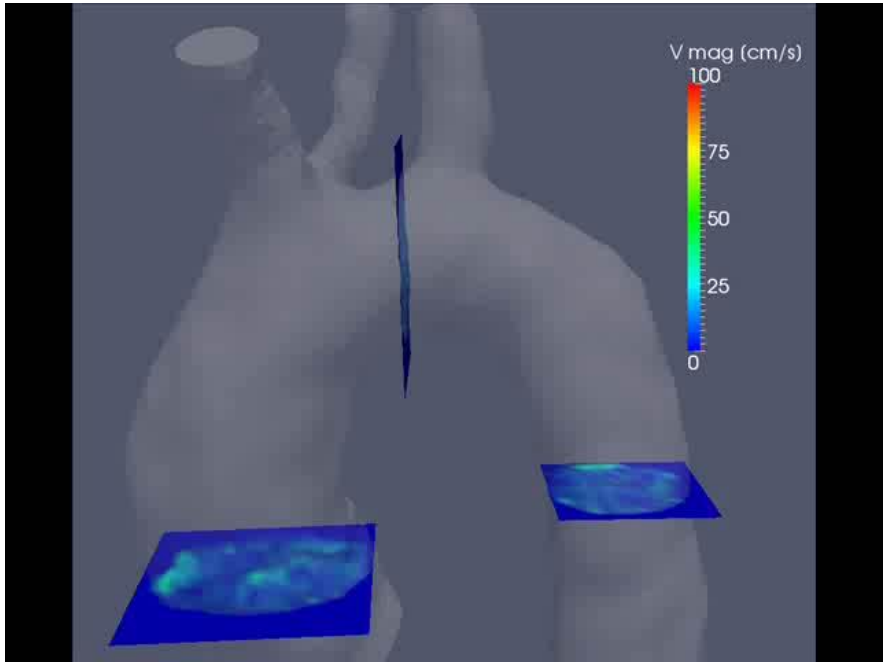

Compared to:

- measured profile, normal component
- developed profile
- plug profile

[Morbiducci et al., 2013]

Results – Outlet BCs strategies

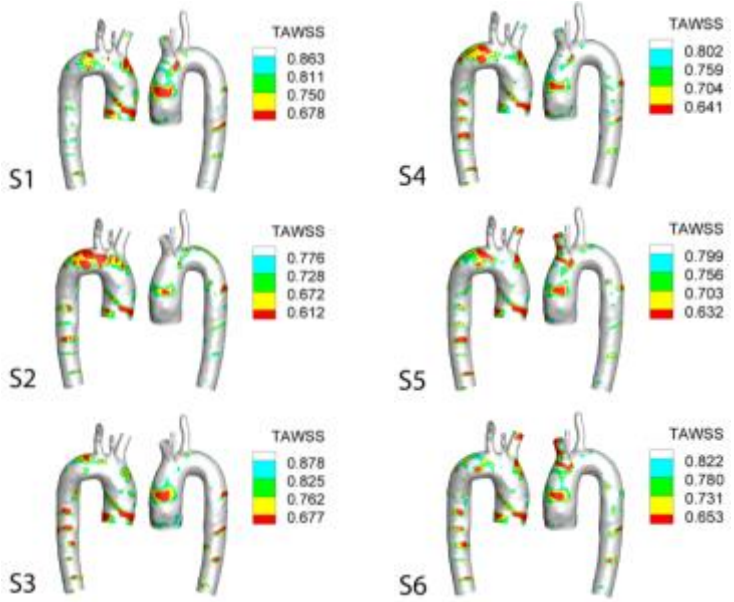

Differences in TAWSS up to **49%**

Major differences: downstream of the supra-aortic vessels due to different **suction conditions**.

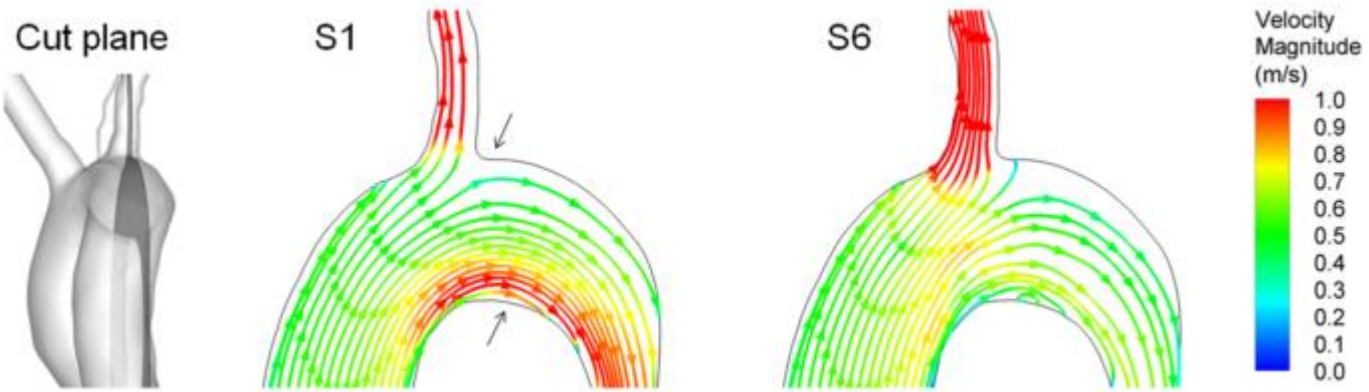

[Gallo et al., 2012]

Results - Measured velocity profiles

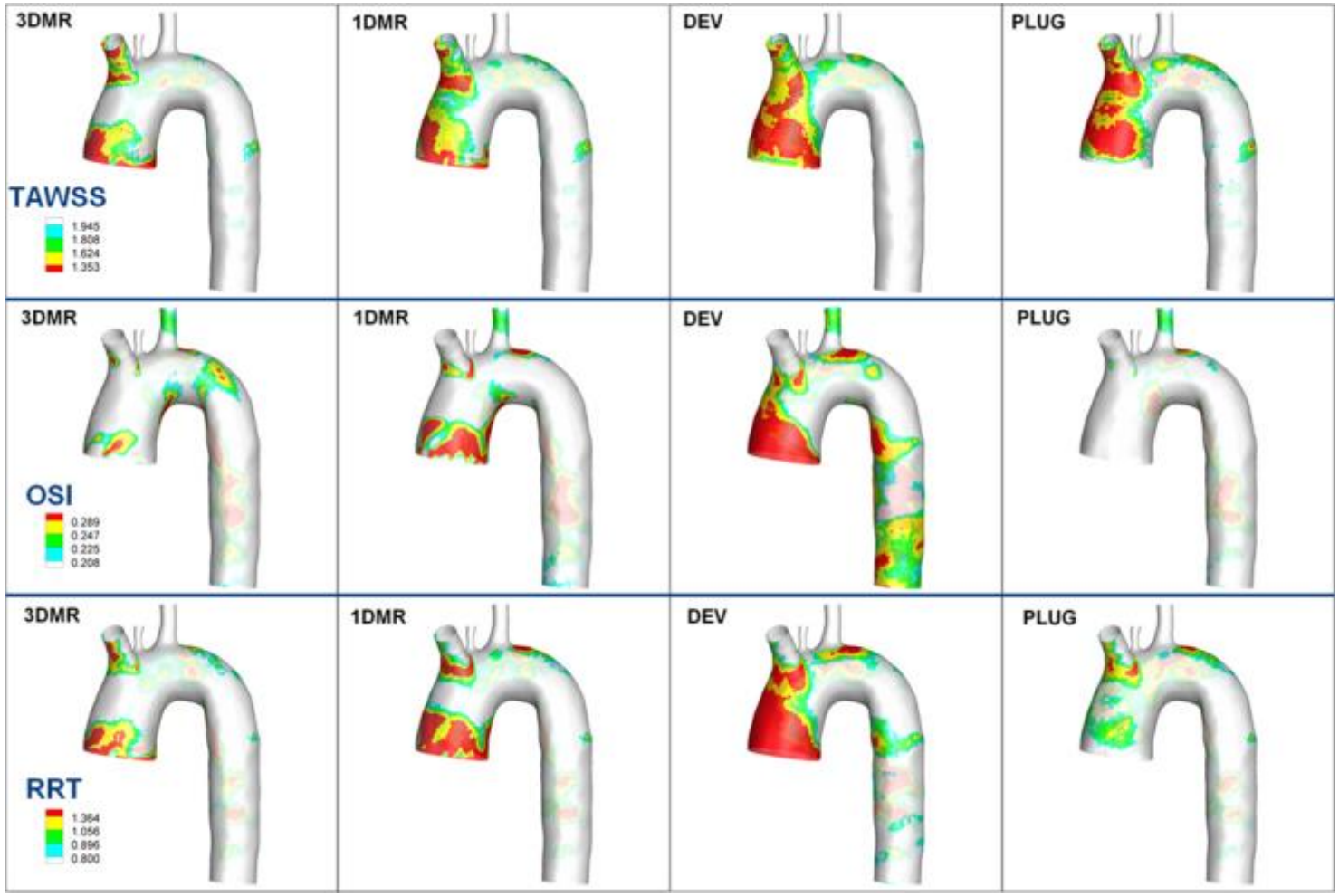

[Morbiducci et al., 2013]

Results - Measured velocity profiles

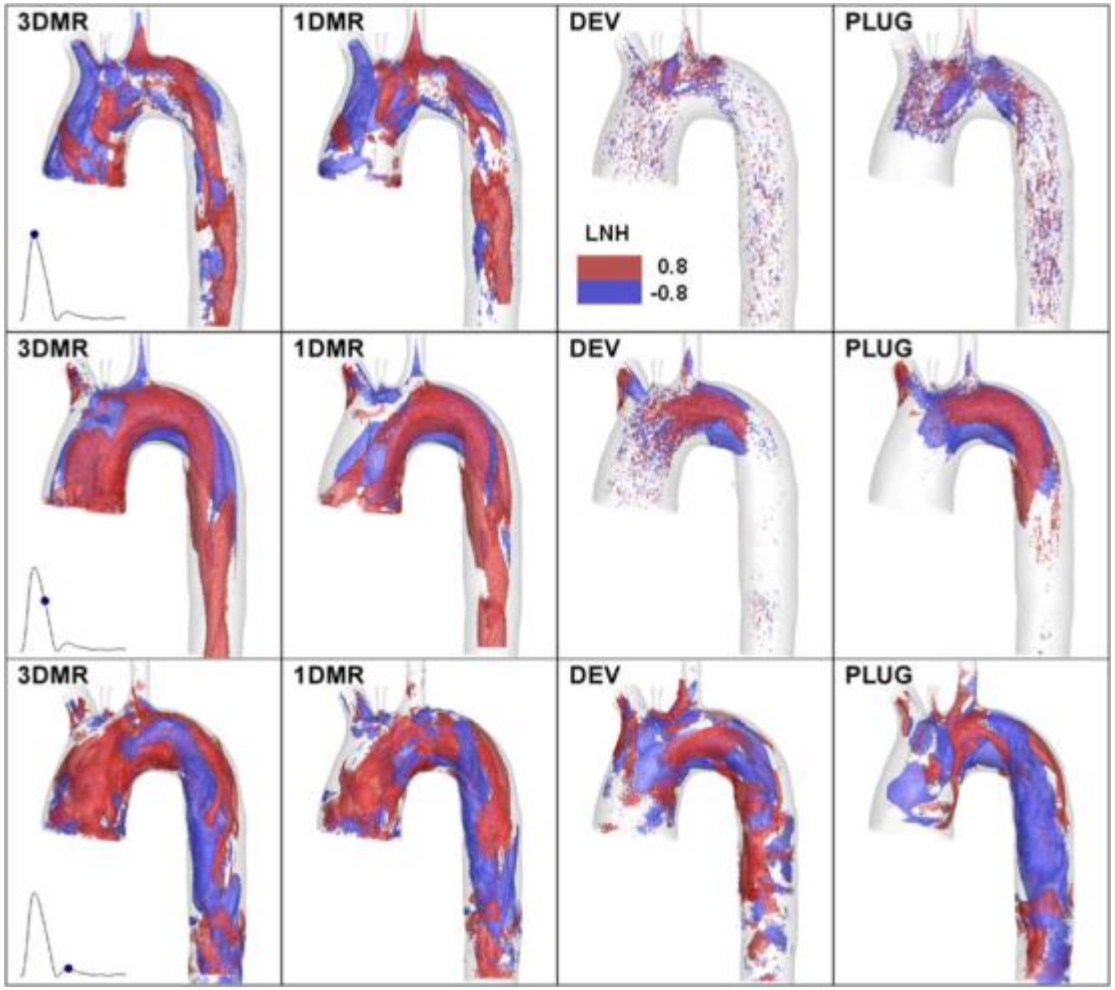

[Morbiducci et al., 2013]

Conclusions

- Different BCs schemes influence **flow separation and reattachment** and as a consequence WSS-based descriptors;
- A proper distribution of total flow is needed.
- **Assumptions on idealized velocity profiles largely affect WSS descriptors and bulk flow**.
- Need of fully personalized, subject-specific analysis of the aorta hemodynamics, with respect to simulations based on defective data BCs.

4D Phase Contrast MRI

4D Phase Contrast MRI (PC MRI) allows for **visualization and quantification of large arteries hemodynamics.**

The 4D flow raw data comprises information along all three spatial dimension, **three velocity directions**, and **time** in the cardiac cycle.

A 3D PC-MRI (B, isosurface rendering of the aorta) can be calculated from the 4D flow data to aid visualization (here: systolic 3D streamlines) and placement of analysis planes for retrospective flow quantification (here, flow rates).

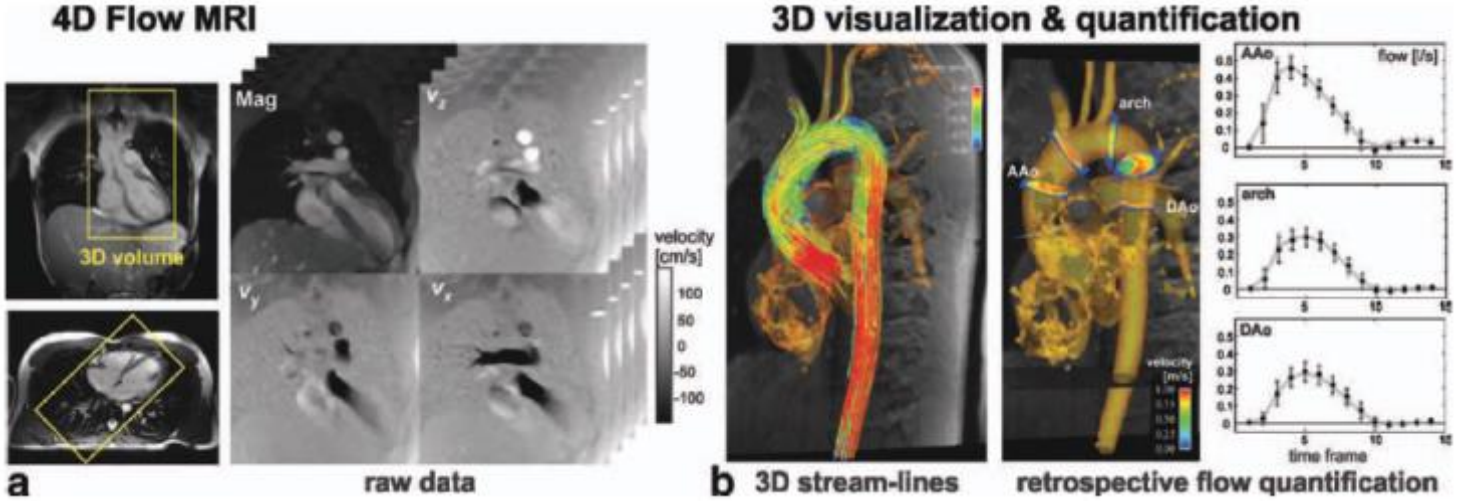

[Markl et al., 2012]

4D Phase Contrast MRI: Moving to bedside?

Allen *et al. Journal of Cardiovascular Magnetic Resonance* 2013, **15**(Suppl 1):P32
http://www.jcmr-online.com/content/15/S1/P32

Journal of Cardiovascular Magnetic Resonance

POSTER PRESENTATION Open Access

Incorporating time-resolved three-dimensional phase contrast (4D flow) MRI in clinical workflow: initial experiences at a large tertiary care medical center

Bradley D Allen*, Alex J Barker, Keyur Parekh, Lewis C Sommerville, Susanne Schnell, Kelly B Jarvis, Maria Carr, James Carr, Jeremy Collins, Michael Markl

From 16th Annual SCMR Scientific Sessions
San Francisco, CA, USA. 31 January - 3 February 2013

4D PC MRI: Aorta Hemodynamics

Blood flow in the aorta is **highly complex**.
In the past massive observations demonstrated:

- Helical flow is **a basic pattern** for almost all the subjects no matter age and gender
- It predominates in areas from the **ascending aorta to the aortic arch**

[Kilner et al., 1993]

However, there is a relative paucity of **in vivo quantitative data** regarding helical blood flow dynamics in the human aorta.

4D PC MRI: Aorta Hemodynamics

Identify common features in physiological aortic bulk flow topology

How

In vivo aortic helical flow quantification in 5 healthy humans by applying **4D PC MRI + tools derived from CFD**, by using a **Lagrangian representation** of the aortic flow.

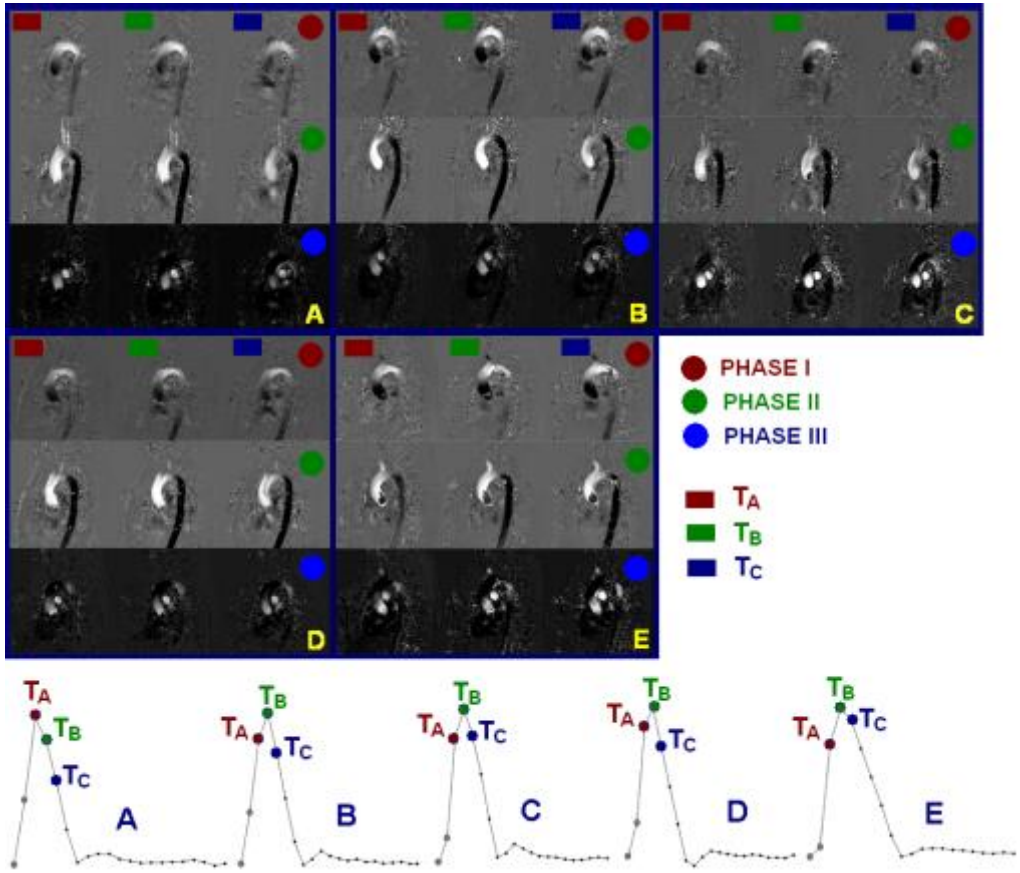

[Morbiducci et al., 2011]

4D Evolution of Aortic Flow

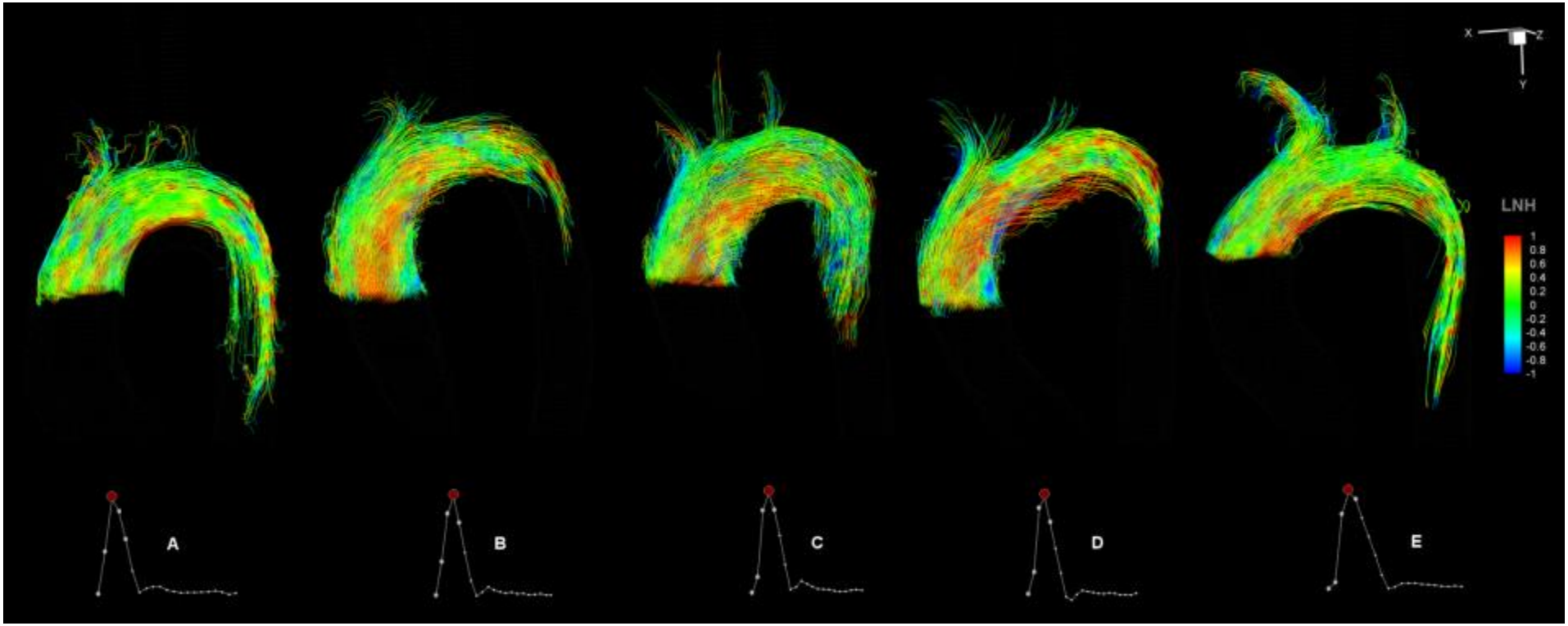

Evolution of the particle set emitted after peak systole is strongly **characterized by helical structures.**

[Morbiducci et al., 2011]

4D Evolution of Aortic Flow

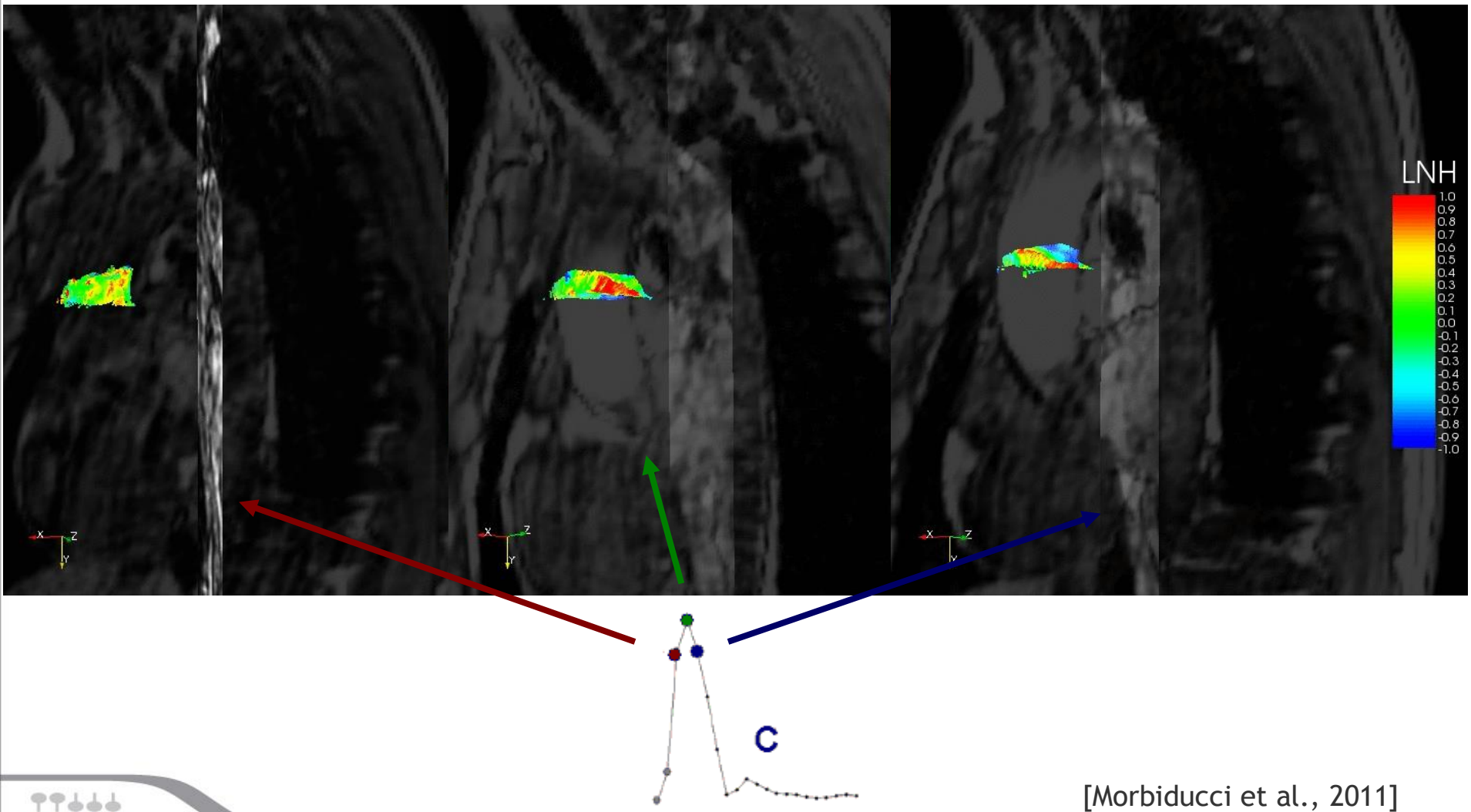

[Morbiducci et al., 2011]

4D Evolution of Aortic Flow

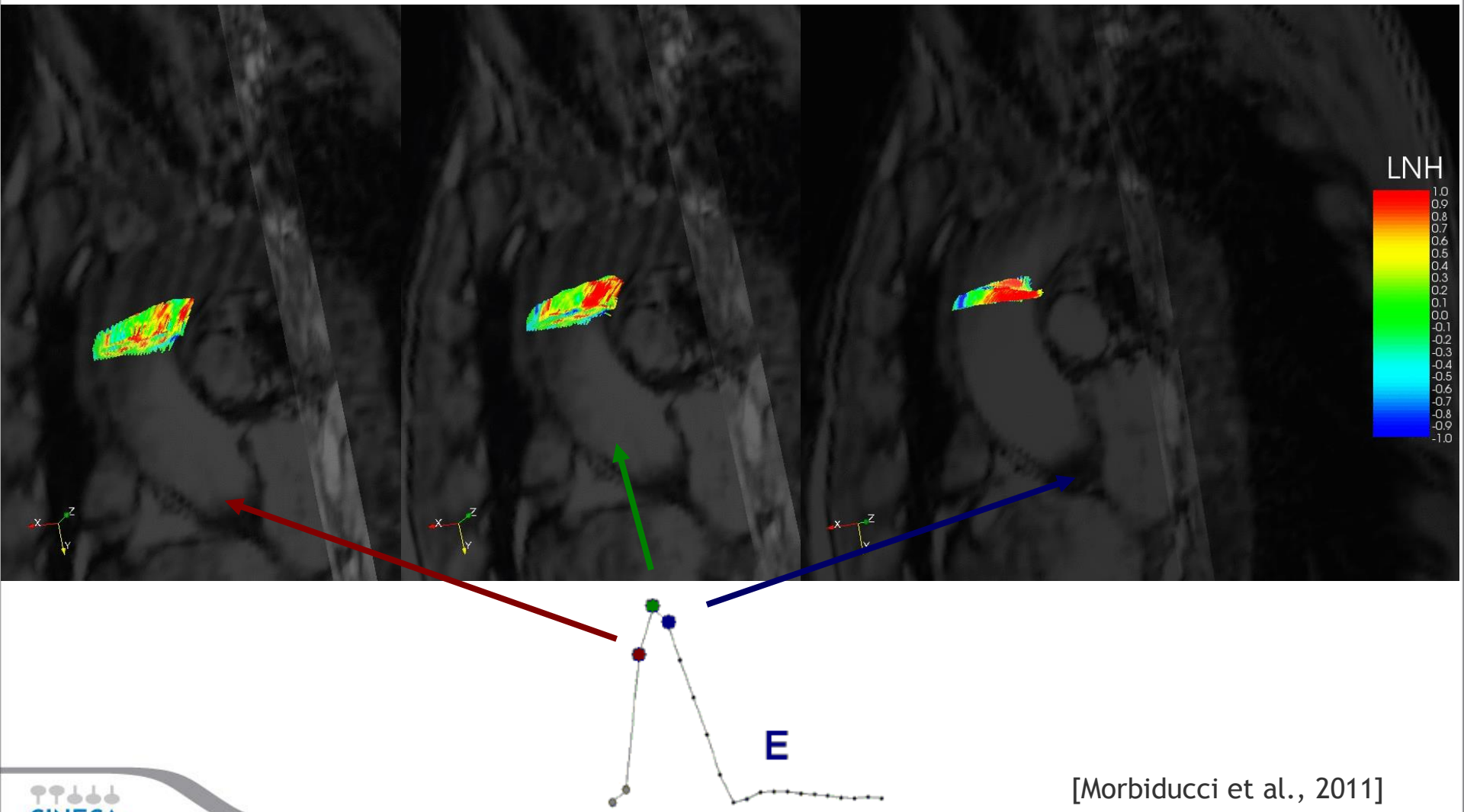

[Morbiducci et al., 2011]

4D Evolution of Aortic Flow

The flow deceleration phase is dominated by the fluid **rotational momentum**, resulting in coherent helical and bi-helical patterns appearing in the ascending aorta.

[Morbiducci et al., 2011]

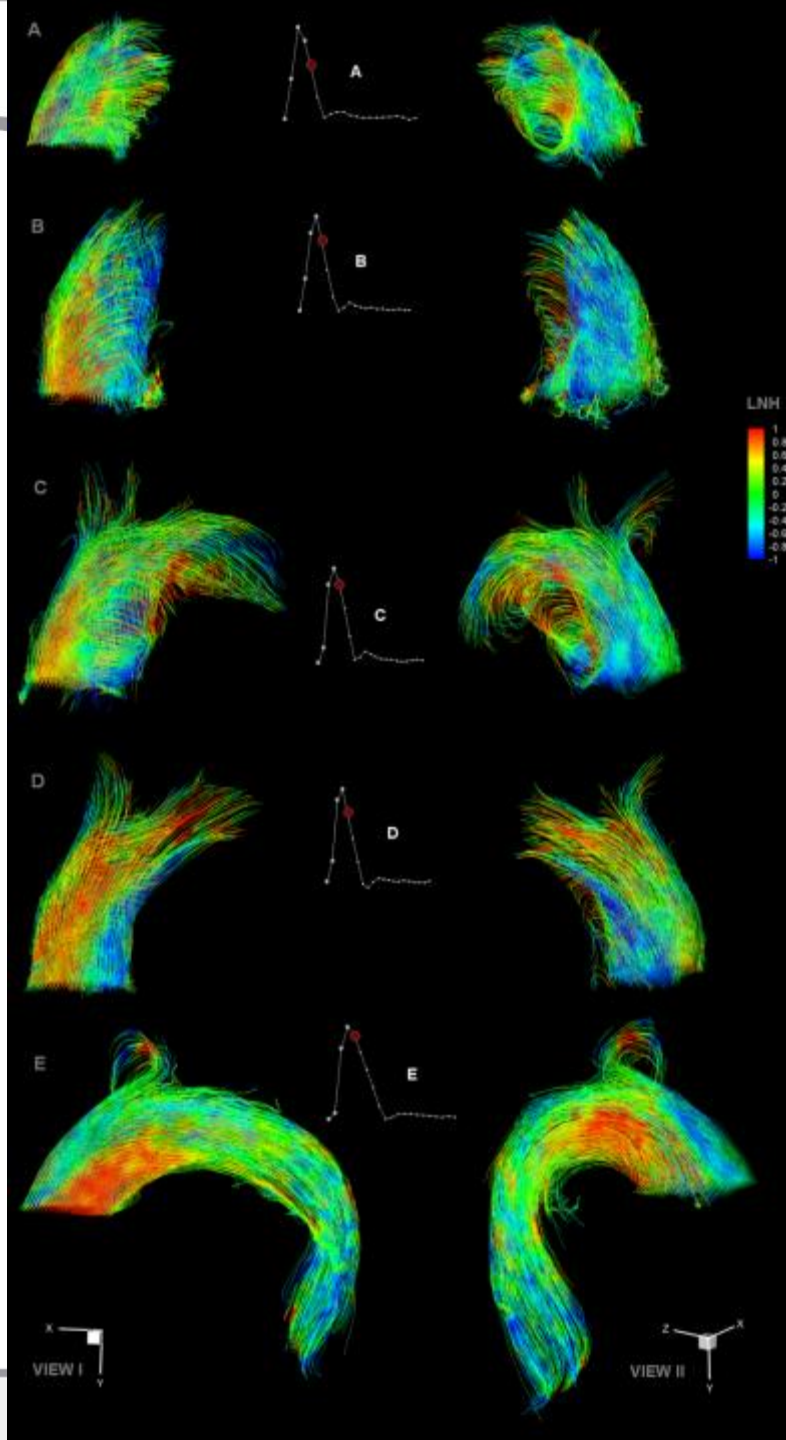

Helicity Quantitative Analysis

INTRAINDIVIDUAL ANALYSIS

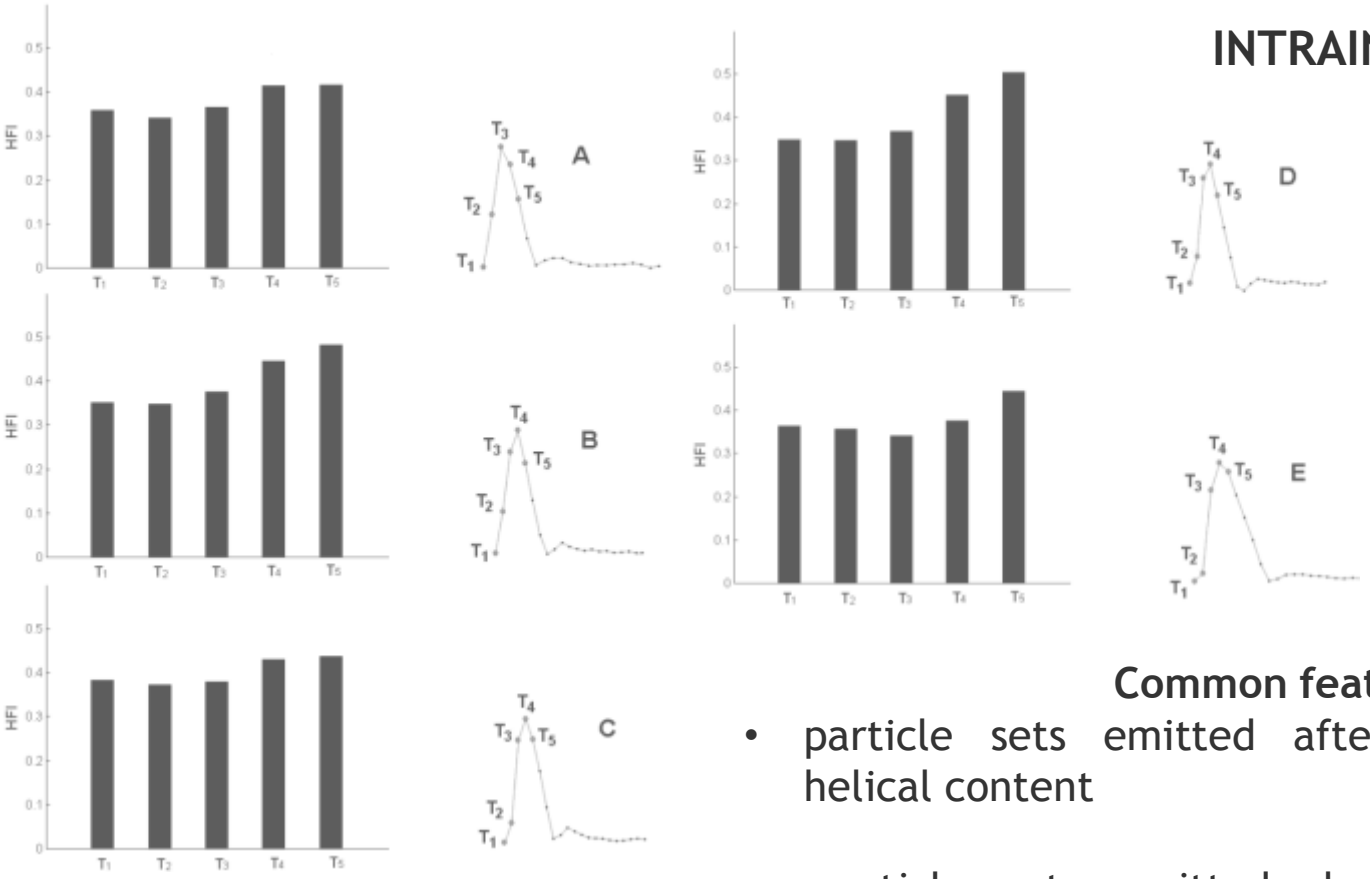

Common features:

- particle sets emitted after peak-systole, highest helical content
- particle sets emitted during acceleration phase characterized by similar trends in HFI values

Bulk flow helical content depends upon the evolution of the flow through the aorta

Conclusions

Incorporation of 4D PC MRI into basic research is a current practice, even if more qualitative than quantitative approach.

Incorporation of 4D PC MRI **into clinical workflow is feasible**.

Technological constraints limit 4D PC MRI translation to clinical practice:
- Scanners spatial/temporal **resolution**
- **Scan time**
- Computational **cost**

In the future, technological evolution will allow for more reliable quantitative analysis (**fusion of image processing and CFD algorithms** applied to in vivo data), to be used for **diagnostic purpose and risk stratification**.

4D PC MRI Applications

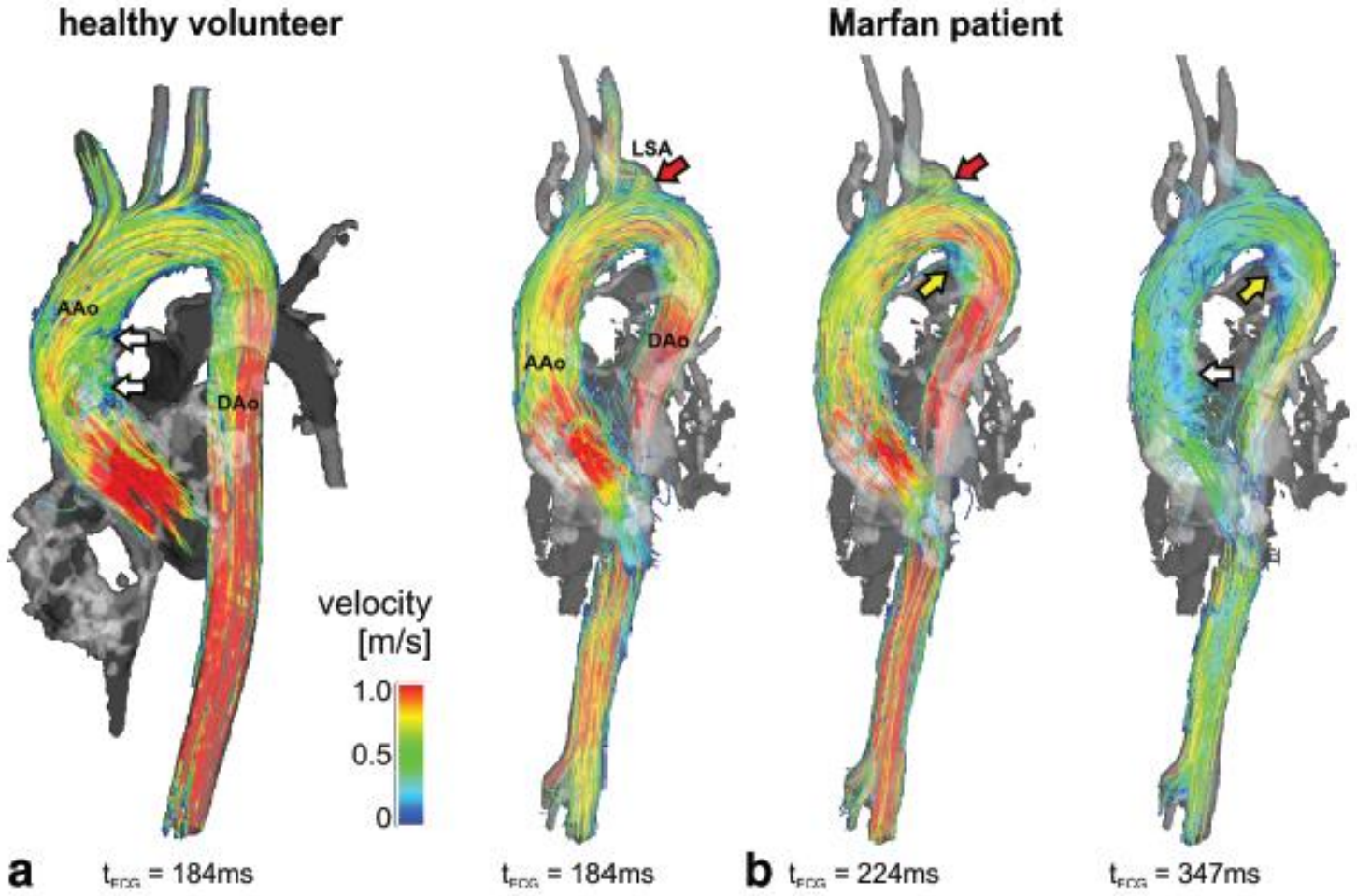

[Geiger et al., 2012]

4D PC MRI Applications

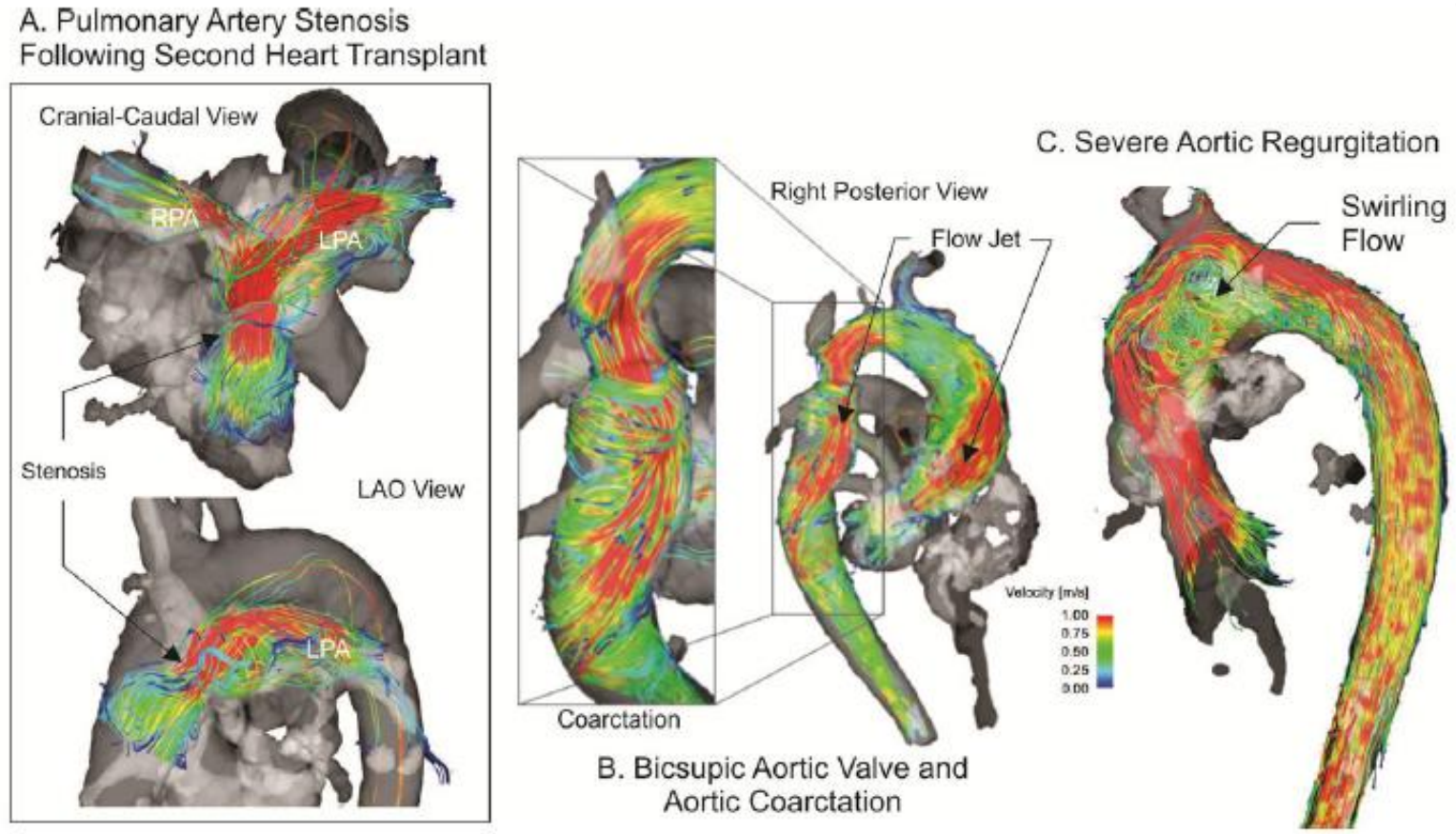

A– Pulmonary artery stenosis B– Aortic coarctation bicuspid valve

C– Aortic regurgitation [Allen et al., 2013]

4D PC MRI Applications

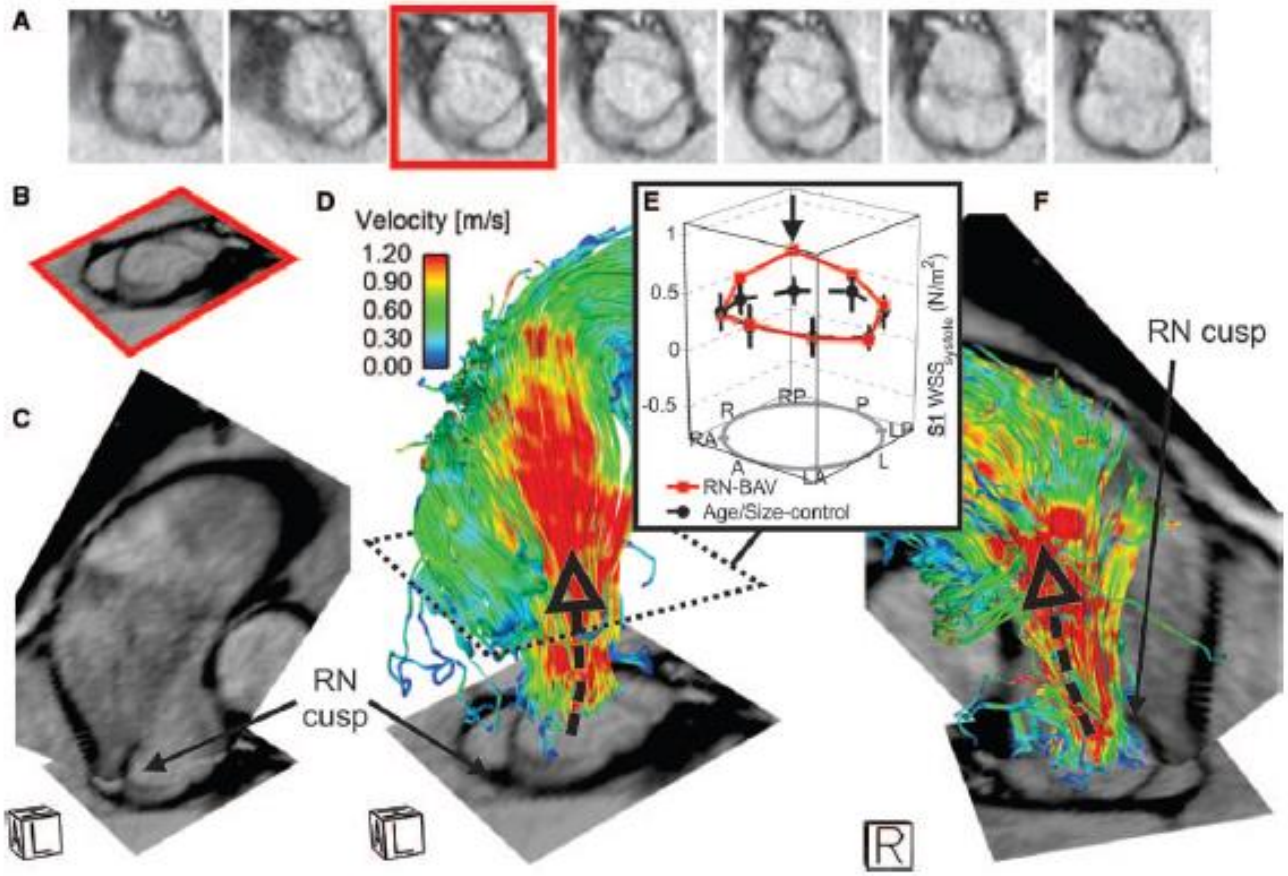

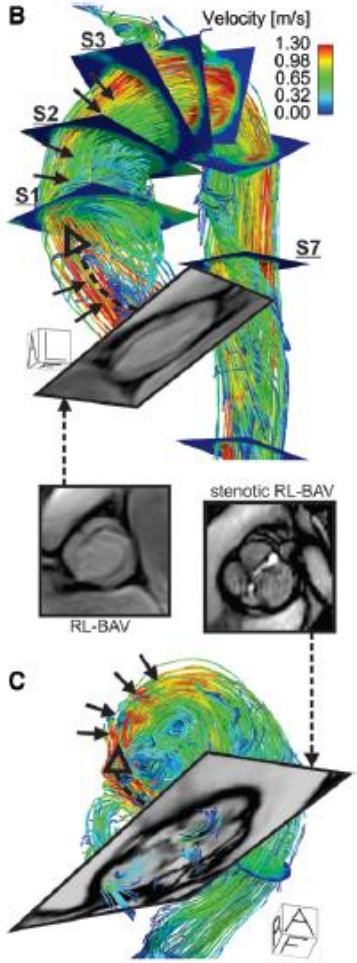

Altered WSS with bicuspid heart valve
[Barker et al., 2010]

4D PC MRI Applications

Distorted aorta

[Markl et al., 2011]

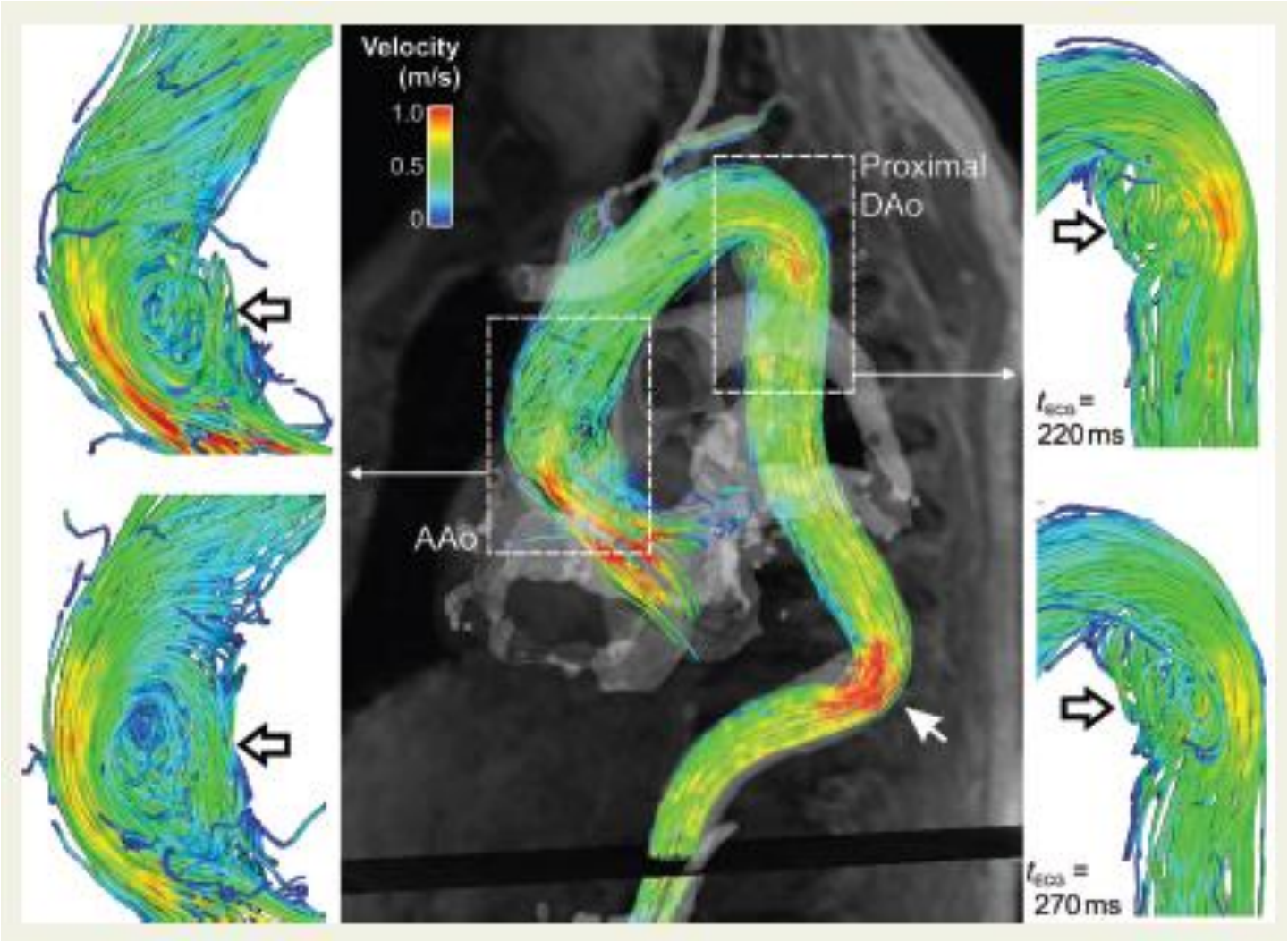

4D PC MRI Applications

Portal vein hemodynamics in patients with cirrosis [Stankovic et al., 2012]

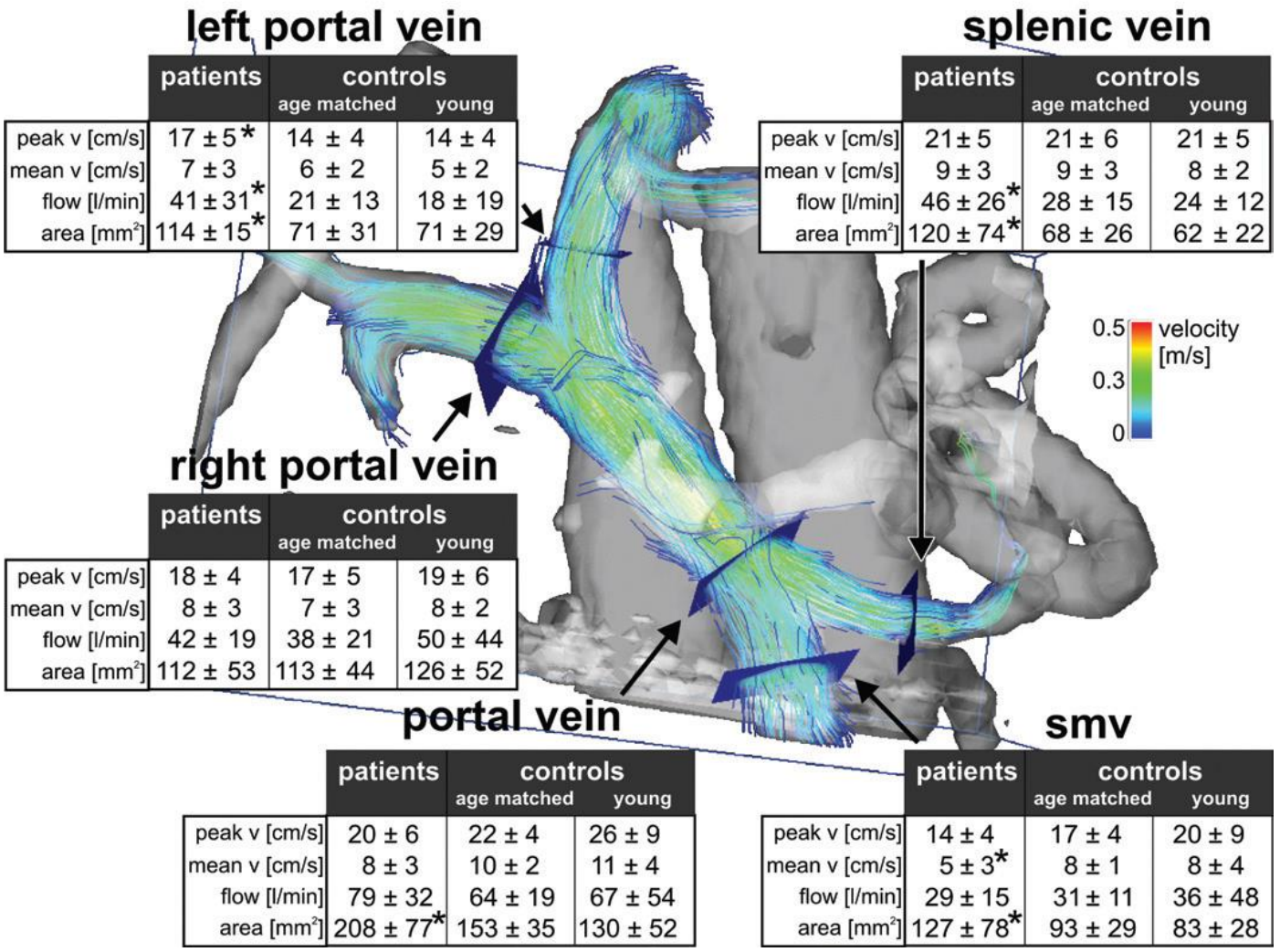

4D PC MRI Applications

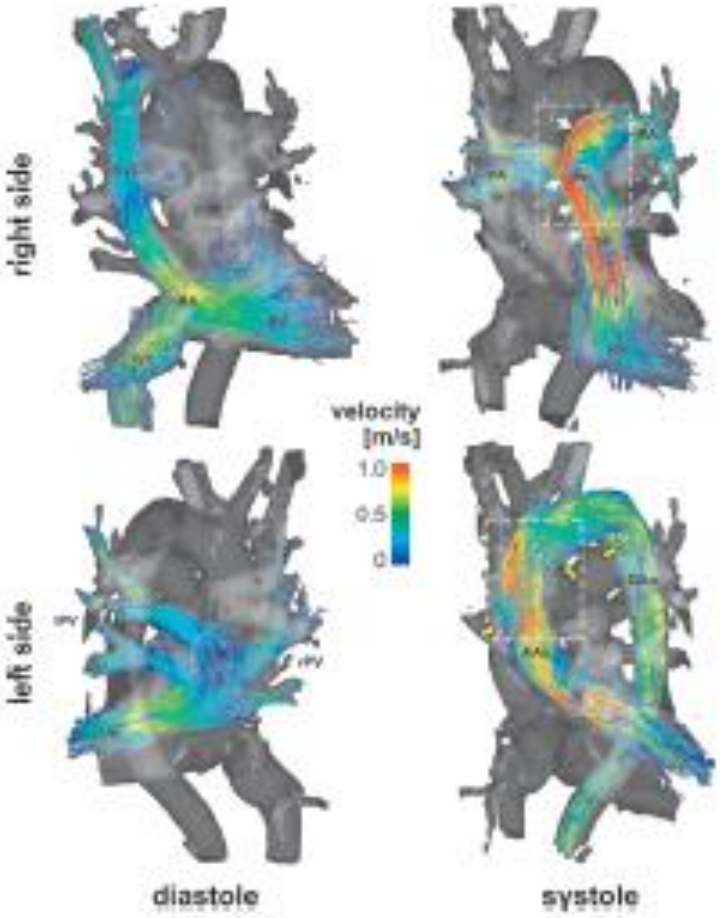

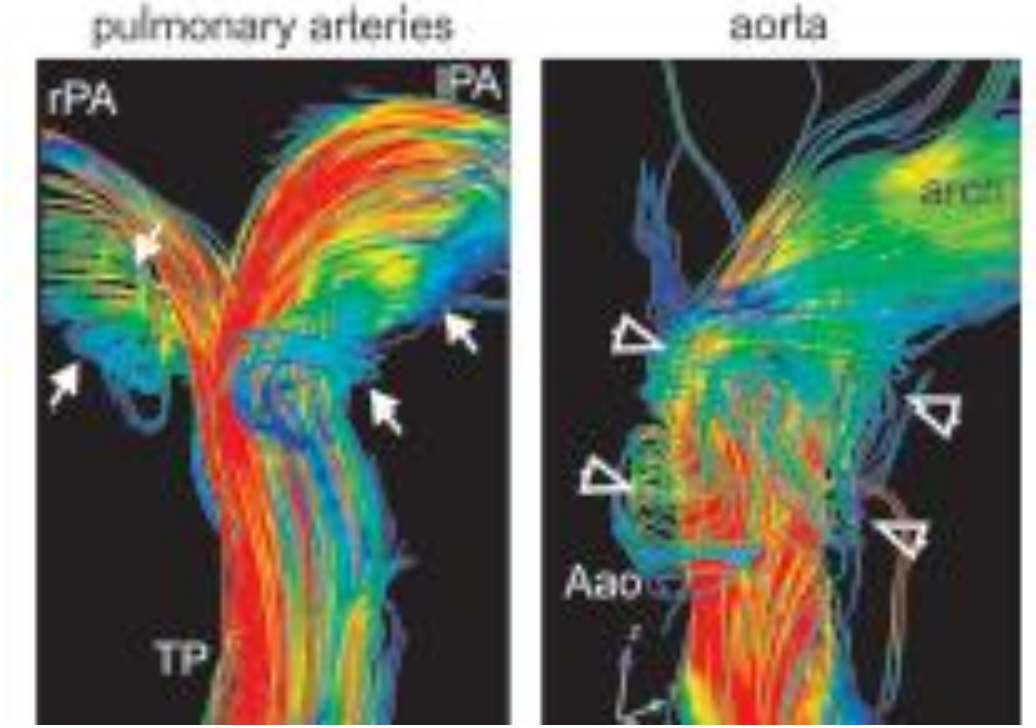

Hemodynamic alterations after heart transplantation

[Markl et al., 2011]

4D PC MRI Applications

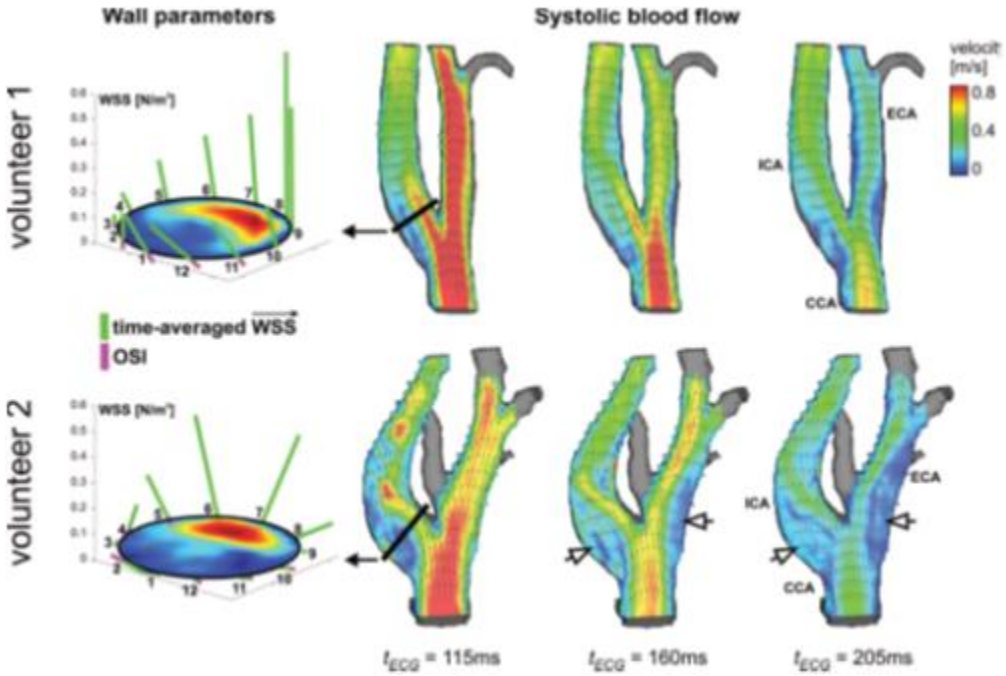

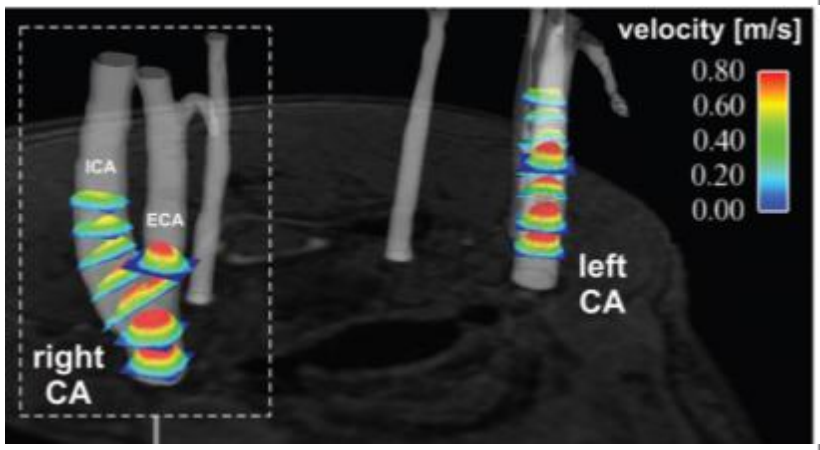

Carotid bifurcation hemodynamics

[Markl et al., 2010]

4D PC MRI Measurements - Caveat

- **They show poor sensitivity to low values of velocity** (only partially overcome by setting multiple velocity encoding).

- Averaging of the measurement in space and time.

- **They are restricted by a spatial resolution between 1.4mm and 2.4mm:** WSS underestimation of one order of magnitude with respect to CFD [Frydrychowicz et al., 2011].

- Difficulty of lumen edge definition.

↓

4D PC MRI measurements are reliable for bulk flow quantities, while for WSS several limitations affect the accuracy of the results.

[Frydrychowicz et al., 201; Boussel et al., 2009, Gallo et al., 2013]

Summary

- Blood flow data contain **valuable information for diagnosis, prognosis, and risk assessment of cardiovascular diseases**. Conventional inspection is insufficient to extract useful information. Thus, comprehensive visualization techniques are necessary to effectively communicate blood-flow dynamics and facilitate the analysis.

- Hemodynamics descriptors are used to **visualize disturbed flow**, to **perform quantitative comparisons** and to **measure hemodynamic performances** of surgical interventions, device optimization, follow-up studies.

- Effective flow visualizations **facilitates a better understanding of the physical phenomena** and also **open new venues of scientific investigation**.

Selected Publications

- Morbiducci*, U., D. Gallo*, D. Massai, F. Consolo, R. Ponzini, L. Antiga, C. Bignardi, M.A. Deriu, and A. Redaelli. Outflow conditions for image-based haemodynamic models of the carotid bifurcation. implications for indicators of abnormal flow. J. Biomech. Eng., 132:091005 (11 pages), 2010. * The two authors equally contributed.
- Morbiducci, U., D. Gallo, R. Ponzini, D. Massai, L. Antiga, A. Redaelli, and F.M. Montevecchi. Quantitative analysis of bulk flow in image-based haemodynamic models of the carotid bifurcation: the influence of outflow conditions as test case. Ann. Biomed. Eng. 38(12):3688-3705, 2010.
- Morbiducci U., D. Gallo, D. Massai, R. Ponzini, M.A. Deriu, L. Antiga, A. Redaelli, and F.M. Montevecchi. On the importance of blood rheology for bulk flow in hemodynamic models of the carotid bifurcation. J. Biomech. 44:2427-2438, 2011.
- Gallo, D., G. De Santis, F. Negri, D. Tresoldi, R. Ponzini, D. Massai, M.A. Deriu, P. Segers, B. Verhegghe, G. Rizzo, and U. Morbiducci. On the use of in vivo measured flow rates as boundary conditions for image-based hemodynamic models of the human aorta. implications for indicators of abnormal flow. Ann. Biomed. Eng. 3:729-741, 2012.
- Gallo, D., D.A. Steinman, P.B. Bijari, and U. Morbiducci. Helical flow in carotid bifurcation as surrogate marker of exposure to abnormal shear. J. Biomech. 45:2398-2404.
- Morbiducci, U., R. Ponzini, D. Gallo, C. Bignardi, G. Rizzo. Inflow boundary conditions for image-based computational hemodynamics: impact of idealized versus measured velocity profiles in the human aorta. J. Biomech. 46:102-109, 2013,
- Gallo, D., G. Isu, D. Massai, F. Pennella, M.A. Deriu, R. Ponzini, C. Bignardi, A. Audenino, G. Rizzo, U. Morbiducci, A survey of quantitative descriptors of arterial flows. In: Visualizations of complex flows in biomedical engineering, Springer.

Acknowledgements

Umberto Morbiducci

Franco Maria Montevecchi

David Steinman

Payam Bijari

Raffaele Ponzini

Luca Antiga

Giovanna Rizzo

Alberto Redaelli

Gianluca De Santis

Patrick Segers

Thank you for your attention!

diego.gallo@polito.it